

Article

Not peer-reviewed version

Re-examination of the Effect of Pairing Gaps on Gamow-Teller Strength Distributions and β -decay Rates

[Jameel-Un Nabi](#)^{*}, Muhammad Riaz, Arslan Mehmood

Posted Date: 22 December 2023

doi: 10.20944/preprints202312.1751.v1

Keywords: Gamow-Teller strength; pairing gaps; half-lives; deformed pn-QRPA; β decay rates, partial half lives



Preprints.org is a free multidiscipline platform providing preprint service that is dedicated to making early versions of research outputs permanently available and citable. Preprints posted at Preprints.org appear in Web of Science, Crossref, Google Scholar, Scilit, Europe PMC.

Copyright: This is an open access article distributed under the Creative Commons Attribution License which permits unrestricted use, distribution, and reproduction in any medium, provided the original work is properly cited.

Article

Re-Examination of the Effect of Pairing Gaps on Gamow-Teller Strength Distributions and β -Decay Rates

Jameel-Un Nabi ^{1,*}, Muhammad Riaz ^{2,†} and Arslan Mehmood ¹

¹ University of Wah, Quaid Avenue, Wah Cantt 47040, Punjab, Pakistan

² Department of Physics, University of Jhang, Jhang, Punjab Pakistan; mriaz@uoj.edu.pk

* Correspondence: jameel@uow.edu.pk

† These authors contributed equally to this work.

Abstract: β -decay is one of the key factors to understand the r -process and evolution of massive stars. The Gamow-Teller (GT) transitions drive the β -decay process. We employ the proton-neutron quasiparticle random phase approximation (pn-QRPA) model to calculate terrestrial and stellar β -decay rates for 50 top-ranked nuclei possessing astrophysical significance according to a recent survey [1]. The model parameters of the pn-QRPA model effect the predicated results of β -decay. The current study investigates the effect of nucleon-nucleon pairing gaps on charge-changing transitions and the associated β decay rates. Three different values of pairing gaps, namely TF, 3TF and 5TF, were used in our investigation. It was concluded that both GT strength distributions and half-lives are sensitive to pairing gap values. The 3TF pairing gap scheme, in our chosen nuclear model, resulted in best prediction with around 80% of the calculated half-lives within a factor 10 of the measured ones. The 3TF pairing scheme also led to calculation of biggest β -decay rates in stellar matter.

Keywords: Gamow-Teller strength; pairing gaps; half-lives; deformed pn-QRPA; β decay rates, partial half lives

1. Introduction

The nuclear reactions mediated by weak interactions play crucial role in presupernova evolution of massive stars [2]. The β^\pm decay, electron and positron capture are the fundamental weak interaction processes that occur during the presupernova phases. The β -decay and electron capture are transformations which produce (anti)neutrinos. A change of lepton-to-baryon fraction (Y_e) of the core matter effects the dynamics of collapse and subsequent explosion of the massive stars [3,4]. The sensitivity of core-collapse dynamics depends on time rate of Y_e and entropy of the core material [5]. The weak interaction mediated rates play an important role in stellar processes including hydrostatic burning, pre-supernova evolution in massive stars and nucleosynthesis (s -, p -, and r -) processes [6,7]. The r -process synthesizes half of the elements heavier than iron [7]. The site of r -process remains uncertain to-date [8–10]. Pre-requisites include high neutron densities and core temperatures. The study of stellar weak interaction rates is a key area for investigation due to its significant contribution in understanding of pre-supernova evolution of massive stars. The core-collapse simulation depends on reliable computation of ground- and excited-states Gamow-Teller (GT) strength functions [5]. A substantial species of unstable nuclei are present in the core with varying abundances. Weak interactions of these nuclei in stellar matter may contribute to a better understanding of the complex dynamics of core-collapse. In the recent years, much experimental work has been conducted to study the nuclear properties of exotic nuclei. Since the majority of these nuclei cannot be created under lab conditions, microscopic calculations of stellar weak-decay properties have gained importance in our quest to comprehend stellar processes. Numerous computations have focused on the mechanisms underlying stellar development and nucleosynthesis (e.g., [11–16]). Once an iron core develops in a giant star's later stages of evolution, there is no more fuel available to start a new burning cycle.

Lepton capture and photo-disintegration processes lead to core's increasing instability and eventual collapse. The number of electrons available for pressure support is reduced by electron capture process, whereas degeneracy pressure is enhanced during β decays [17].

With the advancement of computing and new technologies, calculation of ground and excited states GT strength distributions have gained attention of many researchers. The charge-changing reaction rates in stellar environment were estimated using several nuclear models. Fuller, Fowler, and Newman made the first substantial effort to compute the astrophysical rates using the independent particle model (IPM) [18]. To enhance the reliability of their calculation, they took into account the measurable data that was available at the time. Later many other sophisticated nuclear models were used to calculate reduced transition probabilities of GT transitions. Few noticeable mentions include shell model Monte Carlo technique (e.g., [?]), thermal quasi-particle random-phase approximation, QRPA (e.g., [19–21]), large-scale shell model (e.g., [3]), Gross theory (e.g., [13]), density functional theory (e.g., [14]), Hartree-Fock-Bogoliubov method (e.g., [15]) and shell model (e.g., [16]).

The current study investigates the effect of pairing gaps on calculated GT strength functions and the associated β decay rates under terrestrial and stellar conditions. The β -decay properties were studied using the quasiparticle random phase approximation model with a separable multi-shell schematic and separable interaction on top of axially symmetric-deformed mean-field calculation. Previously a similar investigation was performed separately for *sd*- [22] and *fp*-shell nuclei [23,24]. Recently a list of the top 50 electron capturing and β decay nuclei, possessing the largest effect on Y_e for conditions after silicon core burning, was published [1]. This investigation led to the determination of most important weak interaction nuclei in the presupernova evolution of massive stars. To achieve this goal, an ensemble containing 728 nuclei in the mass range of $A = (1-100)$ was considered. The idea was to sort nuclei having the largest effect on Y_e post silicon core burning, by averaging the contribution from each nucleus to \dot{Y}_e (time-rate of change of lepton fraction) over the entire chosen stellar trajectory. In the current project, we specifically focus on the top-ranked 50 β decay nuclei, as per the findings of Ref. [1], and study the effect of pairing gaps on β -decay properties of these nuclei.

Pairing gaps are one of the most important parameters in the pn-QRPA model. It is to be noted that the present investigation includes neutron-neutron and proton-proton pairing correlations, which have only isovector contribution. For the isoscalar part, one has to include the neutron-proton (*np*) pairing correlations, not considered in the present manuscript. The current pn-QRPA model has the limitation of ignoring the *np* pairing effect and incorporation of *np* pairing may be taken as a future assignment. Such kind of calculations were performed earlier by author in Ref. [25], albeit only for $N=Z+2$ nuclei. The conclusions of their study stated that isoscalar interaction behaves in a fashion similar to the tensor force interaction. The calculations of author [25] showed that the tensor force shifts the GT peak to low excitation energies. Incorporation of tensor force may result in lower centroid values of calculated GT strength distributions and could lead to higher values of calculated β decay rates. In order to compensate, the same effect of shifting calculated β strength to lower excitation energies in the current pn-QRPA model was achieved by incorporation of particle-particle forces (see Section 2 of Ref. [26]). The pairing energy of identical nucleons in even-even isotopes can be estimated using a variety of methods based on the masses of neighboring nuclei, but despite the extensive study of the issue, the issue of which relation most closely approximates the pairing interaction is still open for debate [27–30]. We chose to employ three different recipes for calculation of pairing gaps in our investigation. Details follow in the next section.

The paper is organized as follows: The theoretical framework used for calculations, is described in Section 2. Section 3 presents the discussion on our investigation. Finally, the summary and concluding remarks of the present work are presented in Section 4.

2. Formalism

The Hamiltonian of the current pn-QRPA model is given as

$$H^{pn-QRPA} = H^{sp} + V^{pairing} + V_{GT}^{ph} + V_{GT}^{pp}, \quad (1)$$

where H^{sp} , $V^{pairing}$, V_{GT}^{ph} and V_{GT}^{pp} denote the single-particle Hamiltonian, pairing forces for BCS calculation, particle-hole (ph) and particle-particle (pp) interactions for GT strength, respectively. The single-particle eigenfunctions and eigenvalues were computed using the Nilsson model [31]. Other parameters essential for calculation of weak-interaction rates are nuclear deformation, the Nilsson potential parameters (NPP), the Q-values and the pairing gaps. Nuclear deformation parameter (β_2) was determined using the formula

$$\beta_2 = \frac{125(Q_2)}{1.44(A)^{2/3}(Z)}, \quad (2)$$

where Q_2 is the electric quadrupole moment taken from [32]. The NPP were chosen from [33]. Nilsson oscillator constant was taken as $\hbar\omega = 41/A^{+1/3}$ in units of MeV, similar for neutrons and protons. Q-values were determined using the recent mass compilation [34].

The pairing gaps between nucleons were chosen using three different formulae. The first formula is most often used in literature [26,35,36]. It has the same value for neutron-neutron and proton-proton pairing. It is given by

$$\Delta_{nn} = \Delta_{pp} = 12/\sqrt{A}. \quad (3)$$

This is the traditionally used formula for calculation of pairing gaps. The second formula contains three terms and is based on separation energies of neutrons and protons. It is given by

$$\Delta_{nn} = \frac{1}{8}(-1)^{A-Z+1}[2S_n(A+1, Z) - 4S_n(A, Z) + 2S_n(A-1, Z)] \quad (4)$$

$$\Delta_{pp} = \frac{1}{8}(-1)^{1+Z}[2S_p(A+1, Z+1) - 4S_p(A, Z) + 2S_p(A-1, Z-1)]. \quad (5)$$

The third recipe contains 5 terms and is a function of the binding energies of the nucleons. It is given by

$$\Delta_{nn} = \frac{1}{16}[2B(Z, N-2) - 8B(Z, N-1) + 12B(Z, N) - 8B(Z, N+1) + 2B(Z, N+2)] \quad (6)$$

$$\Delta_{pp} = \frac{1}{16}[2B(Z-2, N) - 8B(Z-1, N) + 12B(Z, N) - 8B(Z+1, N) + 2B(Z+2, N)]. \quad (7)$$

The values of binding energies were taken from Ref. [37]. Henceforth in this text, we will refer to the first formula of pairing gaps as TF (one-term or traditional formula), the second as 3TF (three-term formula) and the last formula as 5TF (five-term formula).

In our pn-QRPA model, charge-changing transitions were defined by phonon creation operators. The pn-QRPA phonons were given as

$$A_{\omega}^{+}(\mu) = \sum_{pn} (X_{\omega}^{pn}(\mu)a_p^{+}a_n^{+} - Y_{\omega}^{pn}(\mu)a_n a_{\bar{p}}). \quad (8)$$

The summation was taken on all the p-n pairs having $\mu = (m_p - m_n) = 0, \pm 1$, where m_n (m_p) represents the third component of angular momentum of neutron (proton). The $a_{n(p)}^{+}$ is the creation operator of a quasi-particle (q.p) state of neutron (proton). \bar{p} represents the time reversed state of p . The ground level of the theory with respect to the QRPA phonons was considered as the vacuum, $A_{\omega}(\mu)|QRPA\rangle = 0$. The excitation energies (ω) and amplitudes (X_{ω}, Y_{ω}) of phonon operator were obtained by solving

the RPA equation. Detailed solution of RPA matrix equation can be seen from Refs. [38,39]. The stellar β decay rates from the n^{th} parent state to m^{th} daughter level was calculated using

$$\lambda_{nm}^{\beta} = \ln 2 \frac{f_{nm}(T, \rho, E_f)}{(ft)_{nm}}. \quad (9)$$

The term $(ft)_{nm}$ is linked to the reduced transition probabilities (B_{nm}) of Fermi and GT transitions

$$(ft)_{nm} = D/B_{nm}, \quad (10)$$

where

$$B_{nm} = (g_A/g_V)^2 B(GT)_{nm} + B(F)_{nm}. \quad (11)$$

The constant D value was chosen as 6143 s [40] and g_A/g_V was taken as -1.254. The reduced Fermi and GT transition probabilities were explicitly determined using

$$B(F)_{nm} = \frac{1}{2J_n + 1} \langle m \parallel \sum_k \tau_{-}^k \parallel n \rangle^2 \quad (12)$$

$$B(GT)_{nm} = \frac{1}{2J_n + 1} \langle m \parallel \sum_k \tau_{-}^k \vec{\sigma}^k \parallel n \rangle^2, \quad (13)$$

where $\vec{\sigma}^k$ and τ_{-}^k denote the spin and the isospin lowering operators, respectively. For the construction of daughter and parent excited states and calculation of nuclear matrix elements, we refer to [41]. For details on solution of Equation 1 we refer to [26,39,41]. The phase space integrals (f_{nm}) over total energy was calculated using

$$f_{nm} = \int_{w_1}^{\infty} w \sqrt{w^2 - 1} (w_m - w)^2 F(+Z, w) (1 - R_-) dw, \quad (14)$$

where we used natural units ($\hbar = m_e = c = 1$). The Fermi functions, $F(+Z, w)$, were estimated as per the prescription given in Ref. [42]. w_m is the total β -decay energy given by

$$w_m = m_p - m_d + E_n - E_m, \quad (15)$$

where E_n and E_m , represent parent and daughter excitation energies, respectively. If the electron emission total energy (w_m) value was larger than -1, then $w_l = 1$, and if $w_m \leq -1$, then $w_m = |w_l|$. R_- is the electron distribution function

$$R_- = \left[\exp\left(\frac{E - E_f}{kT}\right) + 1 \right]^{-1}, \quad (16)$$

where $E = (w - 1)$, E_f denote the kinetic and Fermi energy of the electrons, respectively. k is the Boltzmann constant. As the stellar core temperature rises, there is always a finite chance of occupation of parent excited levels. The total β decay rates were calculated using

$$\lambda^{\beta} = \sum_{nm} P_n \lambda_{nm}^{\beta}, \quad (17)$$

where P_n is the occupation probability of parent excited state following the normal Boltzmann distribution. In Equation 17, the summation was applied on all final and initial states until reasonable convergence in β -decay rates was obtained.

The β decay partial half-lives $t_{1/2}$ from parent ground state were calculated using the relation

$$t_{p(1/2)} = \frac{D}{f_V(Z, E, A) B_F(\omega) + (g_V/g_A)^{-2} f_A(Z, E, A) B_{GT}(\omega)}, \quad (18)$$

where $E = (Q - \omega)$. The integrals of the available phase space for axial vector and vector transitions are denoted as $f_A(Z, A, E)$ and $f_V(Z, A, E)$, respectively. The total β -decay half-lives were computed, including all transition probabilities to the states in the daughter within the Q window.

3. Results and Discussion

The aim of the current study is to re-examine the effect of pairing gaps on charge-changing transitions and associated β -decay rates of 50 top-ranked nuclei bearing astrophysical significance. The nuclei were selected from a recent study by Nabi et al. [1] where a total of 728 nuclei were ranked on the basis of ranking parameter, \hat{R}_p , defined by

$$\hat{R}_p = \left(\frac{\dot{Y}_{e(i)}^{ec(bd)}}{\sum \dot{Y}_{e(i)}^{ec(bd)}} \right)_{0.500 > Y_e > 0.400}, \quad (19)$$

such that the nuclei having highest \hat{R}_p value will contribute most to the time-rate of change of lepton fraction (\dot{Y}_e). As discussed earlier, three different sets of empirically calculated pairing gaps were used in our analysis to investigate the β -decay properties of these nuclei.

The pairing gaps arise from the pairing interaction between nucleons. They have a direct impact on the occupation probabilities of different single-particle states in the nucleus. These probabilities bear consequences for the charge-changing transitions. In general, a larger pairing gap leads to smaller number of nucleons occupying states near the Fermi level. This can contribute to lowering the chances for transitions and may result in redistribution of GT strength to higher excitation energies.

We first display the computed pairing gaps in Figure 1 for the selected 50 nuclei. The upper panels show the neutron-neutron pairing gaps. The proton-proton pairing gaps are displayed in the lower panels. The TF formula (Eq. 3) is only a function of the mass number of the parent nucleus. Nuclear properties of parent and neighbouring nuclei are considered in 3TF formulae (Eq. 4 and Eq. 5). In the 5TF formulae (Eq. 6 and Eq. 7), nuclear properties of two nearest neighbouring nuclei are considered. Difference of more than 0.5 MeV in Δ_{pp} values is noted, between the TF and 3TF schemes, for ^{51}Sc and ^{63}Fe . A difference of similar magnitude is noted for Δ_{pp} between TF and 5TF schemes for the case of $^{64,66}\text{Cu}$. The differences between Δ_{nn} values exceed even more reaching to 0.7 MeV for ^{56}Mn and more than 1 MeV for ^{51}Sc .

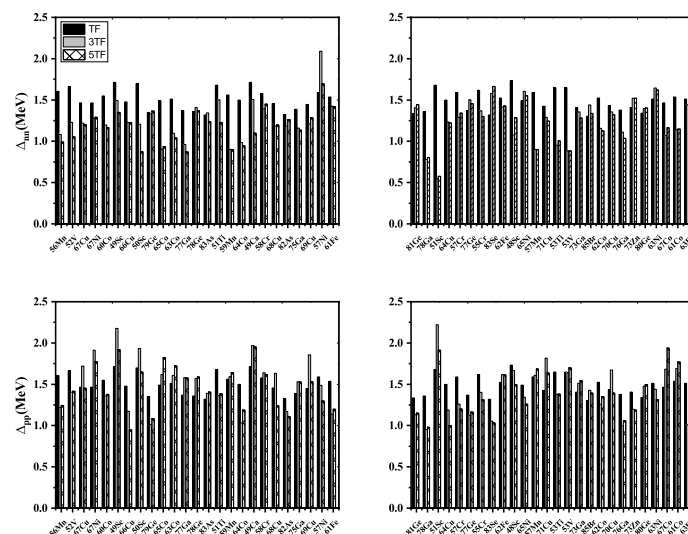
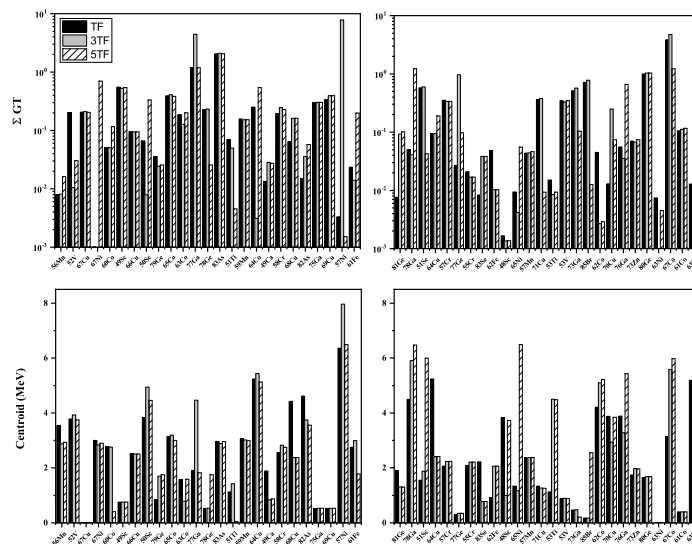


Figure 1. Pairing gap values of the selected 50 nuclei used in the current investigation.

The total strength and centroid values of the calculated GT strength distributions are shown in Figure 2 as a function of pairing gap values. The upper panels show the calculated total GT strength whereas the bottom panels show the computed centroids of the resulting distributions. It is noted from Figure 2 that the total strength and centroid values are sensitive function of the pairing gaps. Orders of magnitude differences are noted for the total GT strength as pairing gap value changes. The effect is more pronounced when the N or Z of the nucleus is a magic number. This includes the nuclei $^{57,63,65,67}\text{Ni}$, ^{85}Br . This was expected as changing pairing gap values would create a bigger impact for closed shell nuclei. It may also be noted that for the case of $^{63,67}\text{Ni}$ (3TF) and ^{67}Ni (TF), the total GT strength are smaller than 10^{-3} and therefore not shown in Figure 2. The average total GT strength calculated by TF, 3TF and 5TF schemes are 0.30, 0.56 and 0.28, respectively. It was concluded that, overall, the 3TF scheme calculated the largest strength values. The placement of centroids changes by an order of magnitude or more as we switch from TF to 3TF schemes. The 5TF has a tendency to move the centroid to higher excitation energies whereas the 3TF places the centroid at much lower energies. The average of all centroids computed by TF, 3TF and 5TF are 2.44 MeV, 2.47 MeV and 2.62 MeV, respectively. More than an order of magnitude difference in the placement of centroid is noted for the case of ^{51}Ti and ^{85}Br (bottom panels of Figure 2). For the case of ^{51}Ti , only one GT transition was calculated by TF and 3TF schemes at energies 1.1 MeV and 1.4 MeV, respectively. The 5TF schemes calculated more fragmentation of the total strength and at low energies (< 0.1 MeV). This explains the placement of centroids at much higher energies for ^{51}Ti employing the pairing gap parameter from TF and 3TF schemes. For the case of ^{85}Br , the 5TF scheme resulted in high-lying GT transitions (between (2-3) MeV). On the other hand, the TF scheme calculated one GT transition at 2.7 MeV, albeit of magnitude 0.00007. All remaining transitions were within 0.5 MeV in daughter states. The 3TF scheme also computed GT transitions within 0.5 MeV in daughter. Consequently, both TF and 3TF placed the centroid at 0.17 MeV in daughter.



Figures 3–6 show the computed branching ratios and partial half-lives as a function of daughter excitation energy for the three selected pairing gaps (TF, 3TF and 5TF) for ^{56}Mn , ^{67}Ni , ^{75}Ga , and ^{78}Ge respectively. These nuclei were selected belonging to odd-odd, even-odd, odd-even and even-even categories from the top-ranked 50 nuclei for the analysis of branching ratios and partial half-lives. Fragmentation of the total GT strength (Figure 2) to low-lying states is altered by changing pairing gap values. The effect is different for different classes of nuclei. For odd-odd cases, Figure 3 shows that low-lying transitions with more fragmentation are produced with 3TF and 5TF schemes. For the magic number nucleus ^{67}Ni , Figure 4 shows that the 5TF scheme result in considerable enhancement of the fragmentation of the GT strength when compared with the other two schemes. The 5TF scheme resulted in low lying transition also for the odd-even nucleus ^{75}Ga as exhibited in Figure 5. For even-even nucleus ^{78}Ge , Figure 6 reveals that the 5TF scheme resulted in lesser fragmentation and high-lying transitions when compared with the TF and 3TF schemes.

The comparison of calculated and measured half-lives for selected top-ranked 50 nuclei is presented in Figure 7. The terrestrial half-lives were calculated using the pn-QRPA model with TF, 3TF and 5TF pairing gap values. The calculated half-life depends on the total strength and distribution of the GT transitions in the daughter states. These two quantities were shown earlier in Figure 2 as a function of the pairing gaps. Three orders of magnitude or more differences in calculated half-life values may be noted from Figure 7. Higher total GT strength values and lower placement of GT centroid result in smaller calculated half-lives. Table 1 shows the accuracy of the current nuclear model using different pairing gap values as one of the input parameters. We defined the ratios of calculated to measured half-lives using the variable y_i

$$y_i = \left\{ \begin{array}{l} \frac{T_{1/2}^{cal}}{T_{1/2}^{exp}} \quad \text{if } T_{1/2}^{cal} \geq T_{1/2}^{exp} \\ \frac{T_{1/2}^{exp}}{T_{1/2}^{cal}} \quad \text{if } T_{1/2}^{cal} < T_{1/2}^{exp} \end{array} \right\} \quad \text{OR} \quad (21)$$

In Table 1, n is the number of half-lives (out of a total of 50 cases) reproduced under the condition given in the first column. The average deviation (\bar{y}) was calculated using

$$y = \frac{1}{n} \sum_{i=1}^n y_i, \quad (22)$$

Table 1 shows that the current model with 3TF pairing gap reproduces 80% (44%) of measured half-lives values within a factor of 10 (2) with an average deviation of 2.42 (1.22). We conclude that the 3TF pairing gap results in calculation of bigger total GT strength and best prediction of half-live values for these top-ranked 50 nuclei.

Because of the crucial importance of these nuclei in stellar environment, we decided to calculate β -decay rates of the selected 50 nuclei as a function of pairing gaps in stellar matter. In general, larger pairing gaps tend to shift the GT centroid to higher excitation energies in daughter. This in turn decreases the β -decay rates. A larger pairing gap leads to smaller number of nucleons occupying states near the Fermi level. This may result in redistribution of GT strength to higher excitation energies. Tables 2–6 show the β decay rates of top-ranked 50 nuclei at selected densities [$\rho Y_e = (10, 10^5, 10^{11}) \text{ g cm}^{-3}$] and temperature [$T = (0.1, 1, 5, 10, 15, 30) \text{ GK}$]. In these tables entries written as $< 10^{-100}$ means that the calculated β -decay rates were less than 10^{-100} s^{-1} . Tables 2–6 display that β decay rates increase as the core temperature increases and decrease as ρY_e increases. The decay rates, for a predetermined density, increase due to accessibility of a large phase space with increasing core temperature. Soaring core temperatures increase the occupation probabilities of parent excited levels, thereby leading to a larger contribution of partial rates from parent excited states to the total rates. As

the stellar core became denser, the electron Fermi energy increases leading to a substantial decrease in the β -decay rates at high stellar density values. Specially at high density ($\rho Y_e = 10^{11} \text{ g cm}^{-3}$), because of choking of the phase space, the β -decay rates tend to zero. It is concluded from Tables 2–6 that the 3TF scheme leads to calculation of biggest stellar β -decay rates. This has a direct correlation with calculation of bigger total GT strength using the 3TF scheme. Table 7 shows the average values of the calculated stellar β -decay rates using different pairing gap values under predetermined physical conditions.

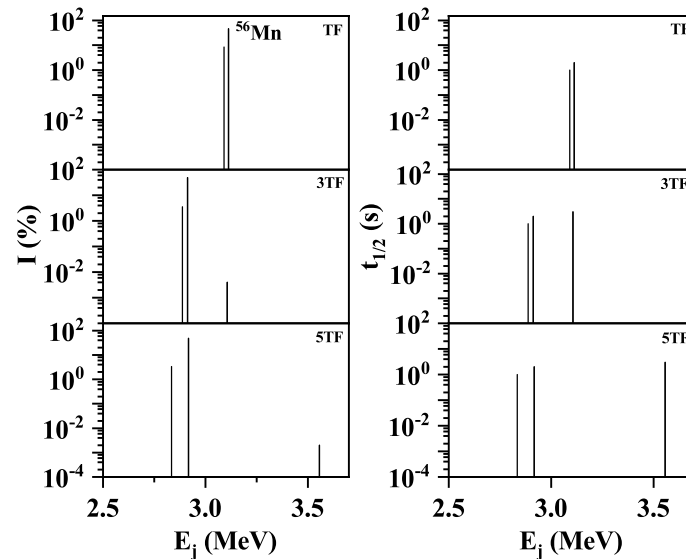


Figure 3. Calculated branching ratios (I) and partial half lives ($t_{1/2}$) for β decay of ^{56}Mn as a function of pairing gaps within the Q -value window.

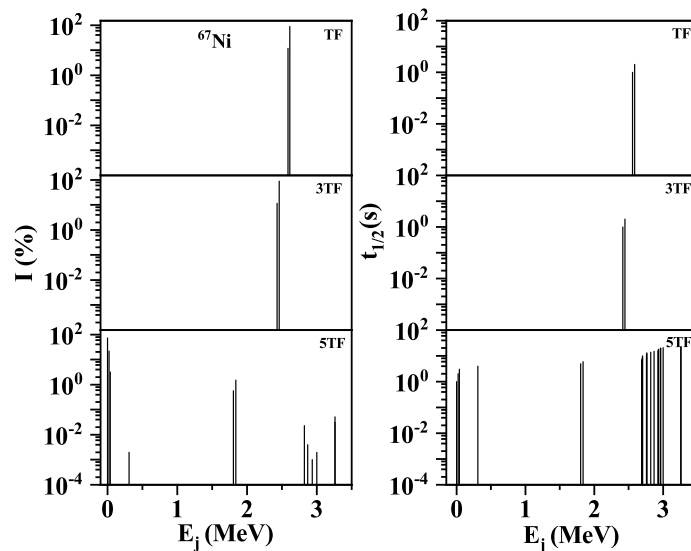


Figure 4. Same as Figure 3 but for ^{67}Ni .

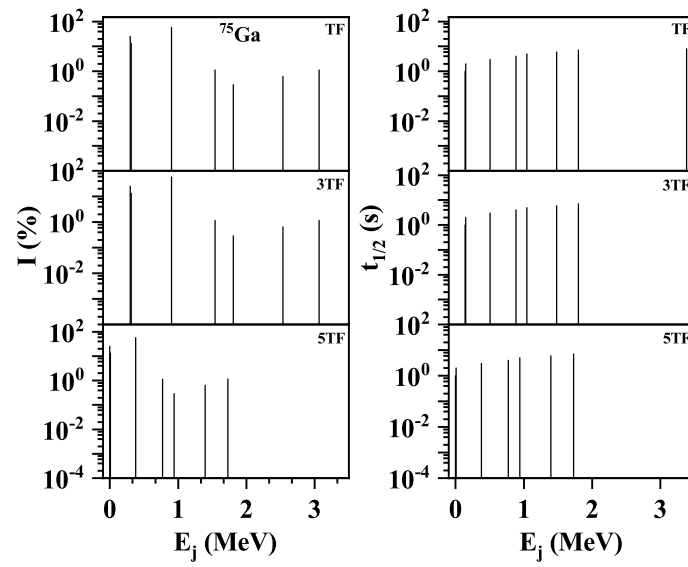


Figure 5. Same as Figure 3 but for ^{75}Ga .

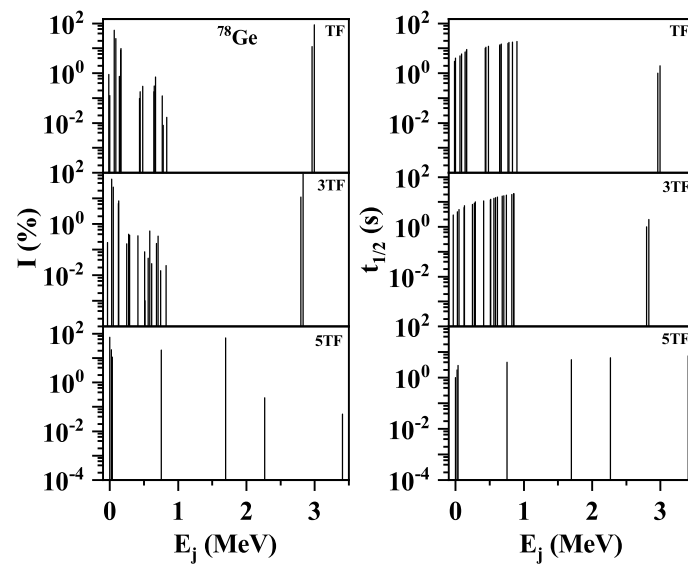


Figure 6. Same as Figure 3 but for ^{78}Ge .

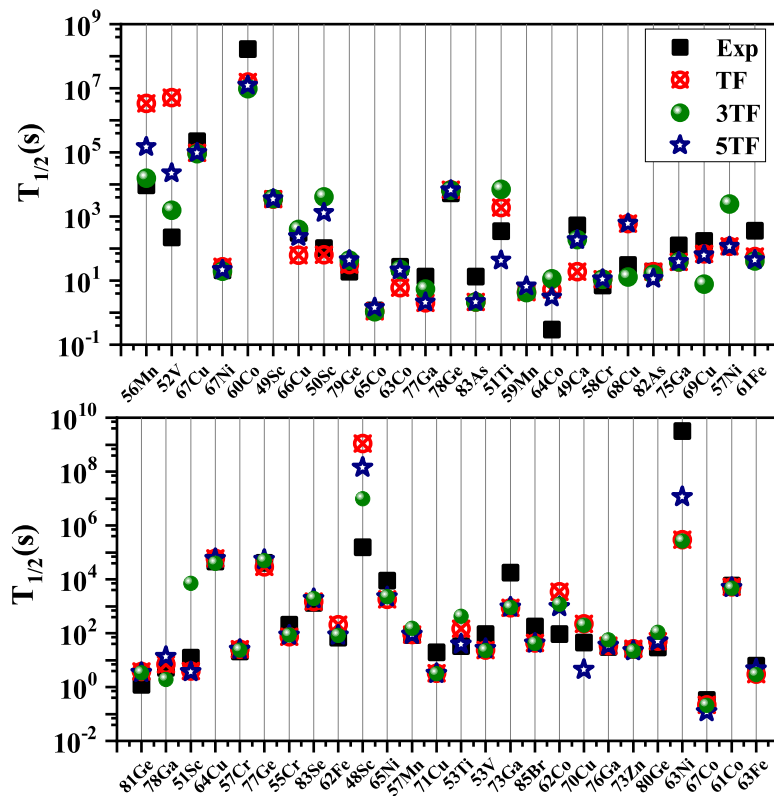


Figure 7. Comparison of measured and predicted half-lives using three different pairing gap values for the selected nuclei. Measured half-lives were taken from Ref. [34].

Table 1. Accuracy of the pn-QRPA model calculated half-lives using three different pairing gaps for the selected 50 top-ranked β -decaying nuclei.

Condition	Pairing Gaps	n	n%	\bar{y}
$\forall y_i \leq 10$	TF	39	78	2.81
	3TF	40	80	2.42
	5TF	36	72	3.18
$\forall y_i \leq 2$	TF	21	42	1.32
	3TF	22	44	1.22
	5TF	18	36	1.42

Table 2. Comparison of calculated stellar β decay rates for $^{48-51}\text{Sc}$, ^{49}Ca , $^{51,53}\text{Ti}$, $^{52,53}\text{V}$, ^{55}Cr and ^{56}Mn as a function of pairing gap values. The stellar core temperature is given in units of GK and densities in units of $g\text{cm}^{-3}$.

Nuclei	T	$\rho=10^1$			$\rho=10^5$			$\rho=10^{11}$		
		TF	3TF	STF	TF	3TF	STF	TF	3TF	STF
^{48}Sc	0.1	8.65×10^{-36}	8.24×10^{-34}	2.56×10^{-36}	7.71×10^{-36}	8.09×10^{-34}	2.49×10^{-36}	$< 10^{-100}$	$< 10^{-100}$	$< 10^{-100}$
	1	3.13×10^{-08}	1.35×10^{-06}	3.85×10^{-07}	2.99×10^{-08}	1.33×10^{-06}	3.80×10^{-07}	$< 10^{-100}$	$< 10^{-100}$	$< 10^{-100}$
	5	1.13×10^{-04}	1.16×10^{-03}	5.36×10^{-04}	1.13×10^{-04}	1.16×10^{-03}	5.36×10^{-04}	8.02×10^{-26}	1.42×10^{-24}	4.13×10^{-25}
	10	5.57×10^{-03}	1.12×10^{-02}	1.03×10^{-02}	5.57×10^{-03}	1.12×10^{-02}	1.03×10^{-02}	2.59×10^{-13}	1.00×10^{-12}	6.55×10^{-13}
	15	3.52×10^{-02}	7.41×10^{-02}	7.23×10^{-02}	3.52×10^{-02}	7.41×10^{-02}	7.23×10^{-02}	5.26×10^{-09}	1.54×10^{-08}	1.24×10^{-08}
	30	2.44×10^{-01}	6.11×10^{-01}	5.74×10^{-01}	2.44×10^{-01}	6.11×10^{-01}	5.74×10^{-01}	1.44×10^{-04}	3.91×10^{-04}	3.50×10^{-04}
^{49}Ca	0.1	1.66×10^{-04}	1.55×10^{-04}	1.53×10^{-04}	1.66×10^{-04}	1.55×10^{-04}	1.53×10^{-04}	$< 10^{-100}$	$< 10^{-100}$	$< 10^{-100}$
	1	3.65×10^{-03}	4.18×10^{-03}	8.47×10^{-04}	3.65×10^{-03}	4.18×10^{-03}	8.47×10^{-04}	3.78×10^{-97}	6.31×10^{-97}	2.34×10^{-97}
	5	5.85×10^{-02}	3.61×10^{-02}	2.25×10^{-02}	5.85×10^{-02}	3.61×10^{-02}	2.25×10^{-02}	5.47×10^{-21}	4.04×10^{-21}	4.07×10^{-21}
	10	3.84×10^{-01}	2.55×10^{-01}	2.43×10^{-01}	3.84×10^{-01}	2.55×10^{-01}	2.43×10^{-01}	1.14×10^{-10}	9.12×10^{-11}	8.73×10^{-11}
	15	$1.26 \times 10^{+00}$	9.98×10^{-01}	9.68×10^{-01}	$1.26 \times 10^{+00}$	9.98×10^{-01}	9.68×10^{-01}	5.36×10^{-07}	6.79×10^{-07}	4.58×10^{-07}
	30	$6.14 \times 10^{+00}$	$1.22 \times 10^{+01}$	$5.50 \times 10^{+00}$	$6.14 \times 10^{+00}$	$1.22 \times 10^{+01}$	$5.50 \times 10^{+00}$	5.45×10^{-03}	1.75×10^{-02}	5.13×10^{-03}
^{49}Sc	0.1	1.37×10^{-38}	9.35×10^{-42}	5.93×10^{-40}	1.36×10^{-38}	9.25×10^{-42}	5.86×10^{-40}	$< 10^{-100}$	$< 10^{-100}$	$< 10^{-100}$
	1	7.19×10^{-07}	3.78×10^{-07}	5.85×10^{-07}	7.14×10^{-07}	3.75×10^{-07}	5.81×10^{-07}	$< 10^{-100}$	$< 10^{-100}$	$< 10^{-100}$
	5	8.73×10^{-04}	1.36×10^{-03}	1.03×10^{-03}	8.73×10^{-04}	1.36×10^{-03}	1.03×10^{-03}	3.33×10^{-24}	2.94×10^{-24}	2.78×10^{-24}
	10	5.26×10^{-03}	5.57×10^{-03}	5.22×10^{-03}	5.26×10^{-03}	5.57×10^{-03}	5.21×10^{-03}	1.25×10^{-12}	1.11×10^{-12}	1.01×10^{-12}
	15	5.32×10^{-02}	3.89×10^{-02}	4.06×10^{-02}	5.32×10^{-02}	3.89×10^{-02}	4.06×10^{-02}	1.63×10^{-08}	1.60×10^{-08}	1.15×10^{-08}
	30	6.81×10^{-01}	$1.04 \times 10^{+00}$	4.28×10^{-01}	6.79×10^{-01}	$1.04 \times 10^{+00}$	4.28×10^{-01}	4.56×10^{-04}	9.98×10^{-04}	2.70×10^{-04}
^{50}Sc	0.1	6.19×10^{-04}	1.76×10^{-04}	4.70×10^{-04}	6.05×10^{-04}	1.73×10^{-04}	4.66×10^{-04}	$< 10^{-100}$	$< 10^{-100}$	$< 10^{-100}$
	1	5.68×10^{-04}	1.66×10^{-04}	3.97×10^{-04}	5.62×10^{-04}	1.64×10^{-04}	3.94×10^{-04}	$< 10^{-100}$	$< 10^{-100}$	$< 10^{-100}$
	5	8.20×10^{-03}	8.87×10^{-03}	1.04×10^{-03}	8.18×10^{-03}	8.87×10^{-03}	1.04×10^{-03}	3.06×10^{-23}	7.11×10^{-23}	8.28×10^{-23}
	10	1.06×10^{-01}	9.31×10^{-02}	1.26×10^{-01}	1.06×10^{-01}	9.31×10^{-02}	1.26×10^{-01}	7.89×10^{-12}	1.13×10^{-11}	1.28×10^{-11}
	15	3.61×10^{-01}	3.47×10^{-01}	5.14×10^{-01}	3.61×10^{-01}	3.47×10^{-01}	5.14×10^{-01}	7.21×10^{-08}	9.40×10^{-08}	1.17×10^{-07}
	30	$1.79 \times 10^{+00}$	$1.92 \times 10^{+00}$	$3.04 \times 10^{+00}$	$1.79 \times 10^{+00}$	$1.92 \times 10^{+00}$	$3.04 \times 10^{+00}$	1.19×10^{-03}	1.38×10^{-03}	2.08×10^{-03}
^{51}Sc	0.1	2.74×10^{-04}	1.80×10^{-05}	9.77×10^{-05}	2.67×10^{-04}	1.71×10^{-05}	9.55×10^{-05}	$< 10^{-100}$	$< 10^{-100}$	$< 10^{-100}$
	1	3.00×10^{-04}	2.15×10^{-05}	1.02×10^{-04}	2.96×10^{-04}	2.09×10^{-05}	1.01×10^{-04}	2.81×10^{-90}	2.77×10^{-90}	2.59×10^{-90}
	5	3.16×10^{-02}	1.20×10^{-02}	1.09×10^{-02}	3.16×10^{-02}	1.20×10^{-02}	1.09×10^{-02}	4.68×10^{-20}	3.70×10^{-20}	3.47×10^{-20}
	10	1.60×10^{-01}	9.75×10^{-02}	1.30×10^{-01}	1.60×10^{-01}	9.75×10^{-02}	1.30×10^{-01}	1.28×10^{-10}	7.48×10^{-11}	6.79×10^{-11}
	15	$1.06 \times 10^{+00}$	4.05×10^{-01}	5.71×10^{-01}	$1.06 \times 10^{+00}$	4.04×10^{-01}	5.71×10^{-01}	6.22×10^{-07}	2.37×10^{-07}	2.10×10^{-07}
	30	$8.63 \times 10^{+00}$	$3.14 \times 10^{+00}$	$2.79 \times 10^{+00}$	$8.63 \times 10^{+00}$	$3.14 \times 10^{+00}$	$2.79 \times 10^{+00}$	8.15×10^{-03}	3.33×10^{-03}	2.06×10^{-03}
^{51}Ti	0.1	1.90×10^{-03}	7.80×10^{-04}	3.17×10^{-04}	1.87×10^{-03}	7.69×10^{-04}	3.14×10^{-04}	$< 10^{-100}$	$< 10^{-100}$	$< 10^{-100}$
	1	1.32×10^{-03}	9.08×10^{-04}	6.62×10^{-04}	1.31×10^{-03}	8.99×10^{-04}	6.58×10^{-04}	$< 10^{-100}$	$< 10^{-100}$	$< 10^{-100}$
	5	5.07×10^{-03}	3.89×10^{-03}	3.12×10^{-03}	5.06×10^{-03}	3.89×10^{-03}	3.11×10^{-03}	1.48×10^{-23}	1.35×10^{-23}	1.44×10^{-23}
	10	4.71×10^{-02}	4.47×10^{-02}	4.38×10^{-02}	4.71×10^{-02}	4.47×10^{-02}	4.38×10^{-02}	2.86×10^{-12}	2.91×10^{-12}	3.10×10^{-12}
	15	1.64×10^{-01}	1.87×10^{-01}	1.82×10^{-01}	1.64×10^{-01}	1.87×10^{-01}	1.82×10^{-01}	2.80×10^{-08}	3.53×10^{-08}	3.41×10^{-08}
	30	$8.75 \times 10^{+00}$	$1.95 \times 10^{+00}$	$1.03 \times 10^{+00}$	$8.75 \times 10^{+00}$	$1.95 \times 10^{+00}$	$1.03 \times 10^{+00}$	5.53×10^{-04}	1.37×10^{-03}	6.81×10^{-03}
^{52}V	0.1	1.30×10^{-07}	7.16×10^{-06}	6.22×10^{-06}	6.43×10^{-08}	6.43×10^{-06}	5.62×10^{-06}	$< 10^{-100}$	$< 10^{-100}$	$< 10^{-100}$
	1	2.52×10^{-06}	2.75×10^{-05}	2.82×10^{-05}	2.39×10^{-06}	2.68×10^{-05}	2.74×10^{-05}	$< 10^{-100}$	$< 10^{-100}$	$< 10^{-100}$
	5	6.17×10^{-04}	9.35×10^{-04}	8.30×10^{-04}	6.15×10^{-04}	9.33×10^{-04}	8.30×10^{-04}	1.61×10^{-25}	5.85×10^{-25}	5.22×10^{-25}
	10	1.38×10^{-02}	2.02×10^{-02}	1.95×10^{-02}	1.38×10^{-02}	2.02×10^{-02}	1.95×10^{-02}	2.90×10^{-13}	6.27×10^{-13}	6.08×10^{-13}
	15	5.25×10^{-02}	8.71×10^{-02}	8.89×10^{-02}	5.25×10^{-02}	8.71×10^{-02}	8.89×10^{-02}	4.95×10^{-09}	1.01×10^{-08}	1.04×10^{-08}
	30	2.81×10^{-01}	5.28×10^{-01}	5.70×10^{-01}	2.81×10^{-01}	5.28×10^{-01}	5.69×10^{-01}	1.41×10^{-04}	2.86×10^{-04}	3.08×10^{-04}
^{53}Ti	0.1	2.46×10^{-03}	1.65×10^{-03}	1.63×10^{-03}	2.44×10^{-03}	1.64×10^{-03}	1.62×10^{-03}	$< 10^{-100}$	$< 10^{-100}$	$< 10^{-100}$
	1	3.38×10^{-03}	2.76×10^{-03}	2.76×10^{-03}	3.37×10^{-03}	2.75×10^{-03}	2.75×10^{-03}	3.40×10^{-97}	2.62×10^{-97}	2.72×10^{-97}
	5	4.80×10^{-02}	2.77×10^{-02}	2.88×10^{-02}	4.80×10^{-02}	2.77×10^{-02}	2.88×10^{-02}	1.16×10^{-20}	9.35×10^{-21}	9.53×10^{-21}
	10	5.41×10^{-01}	4.32×10^{-01}	4.39×10^{-01}	5.41×10^{-01}	4.32×10^{-01}	4.39×10^{-01}	1.52×10^{-10}	1.61×10^{-10}	1.60×10^{-10}
	15	$1.55 \times 10^{+00}$	$1.64 \times 10^{+00}$	$1.60 \times 10^{+00}$	$1.55 \times 10^{+00}$	$1.64 \times 10^{+00}$	$1.60 \times 10^{+00}$	6.32×10^{-07}	8.59×10^{-07}	8.00×10^{-07}
	30	$6.34 \times 10^{+00}$	$1.18 \times 10^{+01}$	$7.50 \times 10^{+00}$	$6.34 \times 10^{+00}$	$1.18 \times 10^{+01}$	$7.50 \times 10^{+00}$	5.61×10^{-03}	1.22×10^{-02}	7.28×10^{-03}
^{53}V	0.1	6.52×10^{-03}	4.78×10^{-03}	4.78×10^{-03}	6.47×10^{-03}	4.74×10^{-03}	4.75×10^{-03}	$< 10^{-100}$	$< 10^{-100}$	$< 10^{-100}$
	1	6.52×10^{-03}	4.74×10^{-03}	4.76×10^{-03}	6.49×10^{-03}	4.72×10^{-03}	4.74×10^{-03}	$< 10^{-100}$	$< 10^{-100}$	$< 10^{-100}$
	5	6.61×10^{-03}	4.10×10^{-03}	4.67×10^{-03}	6.61×10^{-03}	4.10×10^{-03}	4.67×10^{-03}	2.18×10^{-23}	1.40×10^{-23}	1.14×10^{23}
	10	2.82×10^{-02}	1.89×10^{-02}	2.06×10^{-02}	2.82×10^{-02}	1.89×10^{-02}	2.06×10^{-02}	2.98×10^{-12}	1.39×10^{-12}	1.25×10^{-12}
	15	2.19×10^{-01}	1.11×10^{-01}	1.15×10^{-01}	2.19×10^{-01}	1.11×10^{-01}	1.15×10^{-01}	4.66×10^{-08}	1.86×10^{-08}	1.70×10^{-08}
	30	$1.82 \times 10^{+00}$	$1.07 \times 10^{+00}$	6.98×10^{-01}	$1.82 \times 10^{+00}$	$1.07 \times 10^{+00}$	6.98×10^{-01}	1.21×10^{-03}	6.93×10^{-04}	4.05×10^{-04}
^{55}Cr	0.1	1.17×10^{-03}	8.39×10^{-04}	7.41×10^{-04}	1.16×10^{-03}	8.32×10^{-04}	7.35×10^{-04}	$< 10^{-100}$	$< 10^{-100}$	$< 10^{-100}$
	1	1.18×10^{-03}	$$							

Table 3. Same as Table 1 but for $^{57,58}\text{Cr}$, $^{57,59}\text{Mn}$, ^{57}Ni , $^{60-63}\text{Co}$ and $^{61-63}\text{Fe}$.

Nuclei	T	$\rho=10^1$			$\rho=10^5$			$\rho=10^{11}$		
		TF	3TF	5TF	TF	3TF	5TF	TF	3TF	5TF
^{57}Cr	0.1	1.04×10^{-06}	6.32×10^{-02}	6.38×10^{-02}	9.23×10^{-07}	6.31×10^{-02}	6.37×10^{-02}	$< 10^{-100}$	$< 10^{-100}$	$< 10^{-100}$
	1	2.25×10^{-06}	7.94×10^{-02}	7.82×10^{-02}	2.20×10^{-06}	7.94×10^{-02}	7.82×10^{-02}	4.11×10^{-97}	8.63×10^{-98}	9.29×10^{-98}
	5	1.35×10^{-02}	1.22×10^{-01}	1.21×10^{-01}	1.35×10^{-02}	1.22×10^{-01}	1.21×10^{-01}	1.46×10^{-20}	2.59×10^{-21}	2.67×10^{-21}
	10	1.36×10^{-01}	3.27×10^{-01}	3.28×10^{-01}	1.36×10^{-01}	3.27×10^{-01}	3.28×10^{-01}	2.04×10^{-10}	4.03×10^{-11}	4.09×10^{-11}
	15	6.87×10^{-01}	8.93×10^{-01}	8.61×10^{-01}	6.87×10^{-01}	8.93×10^{-01}	8.61×10^{-01}	8.39×10^{-07}	2.40×10^{-07}	2.21×10^{-07}
^{57}Mn	30	$4.65 \times 10^{+00}$	$5.45 \times 10^{+00}$	$3.44 \times 10^{+00}$	$4.65 \times 10^{+00}$	$5.45 \times 10^{+00}$	$3.44 \times 10^{+00}$	6.05×10^{-03}	4.50×10^{-03}	2.55×10^{-03}
	0.1	3.12×10^{-03}	2.94×10^{-03}	3.13×10^{-03}	3.08×10^{-03}	2.92×10^{-03}	3.10×10^{-03}	$< 10^{-100}$	$< 10^{-100}$	$< 10^{-100}$
	1	6.95×10^{-03}	6.64×10^{-03}	6.76×10^{-03}	6.90×10^{-03}	6.61×10^{-03}	6.73×10^{-03}	$< 10^{-100}$	$< 10^{-100}$	$< 10^{-100}$
	5	9.93×10^{-03}	9.33×10^{-03}	9.33×10^{-03}	9.93×10^{-03}	9.33×10^{-03}	9.33×10^{-03}	3.46×10^{-24}	2.13×10^{-24}	2.66×10^{-24}
	10	1.63×10^{-02}	1.35×10^{-02}	1.35×10^{-02}	1.63×10^{-02}	1.35×10^{-02}	1.35×10^{-02}	5.85×10^{-13}	3.22×10^{-13}	3.72×10^{-13}
^{57}Ni	15	6.27×10^{-02}	3.58×10^{-02}	3.30×10^{-02}	6.27×10^{-02}	3.58×10^{-02}	3.30×10^{-02}	8.28×10^{-09}	5.64×10^{-09}	3.81×10^{-09}
	30	4.32×10^{-01}	4.30×10^{-01}	1.46×10^{-01}	4.32×10^{-01}	4.30×10^{-01}	1.46×10^{-01}	2.42×10^{-04}	4.06×10^{-04}	7.83×10^{-05}
	0.1	$< 10^{-100}$	$< 10^{-100}$	$< 10^{-100}$	$< 10^{-100}$	$< 10^{-100}$	$< 10^{-100}$	$< 10^{-100}$	$< 10^{-100}$	$< 10^{-100}$
	1	$< 10^{-100}$	3.47×10^{-73}	$< 10^{-100}$	$< 10^{-100}$	3.01×10^{-73}	$< 10^{-100}$	$< 10^{-100}$	$< 10^{-100}$	$< 10^{-100}$
	5	$< 10^{-100}$	5.57×10^{-20}	$< 10^{-100}$	$< 10^{-100}$	5.55×10^{-20}	$< 10^{-100}$	$< 10^{-100}$	2.99×10^{-43}	$< 10^{-100}$
^{58}Cr	10	$< 10^{-100}$	1.93×10^{-13}	$< 10^{-100}$	$< 10^{-100}$	1.93×10^{-13}	$< 10^{-100}$	$< 10^{-100}$	5.40×10^{-25}	$< 10^{-100}$
	15	$< 10^{-100}$	2.93×10^{-11}	$< 10^{-100}$	$< 10^{-100}$	2.93×10^{-11}	$< 10^{-100}$	$< 10^{-100}$	8.45×10^{-19}	$< 10^{-100}$
	30	$< 10^{-100}$	5.16×10^{-09}	$< 10^{-100}$	$< 10^{-100}$	5.16×10^{-09}	$< 10^{-100}$	$< 10^{-100}$	1.60×10^{-12}	$< 10^{-100}$
	0.1	7.13×10^{-02}	7.59×10^{-02}	7.45×10^{-02}	7.10×10^{-02}	7.55×10^{-02}	7.41×10^{-02}	$< 10^{-100}$	$< 10^{-100}$	$< 10^{-100}$
	1	7.13×10^{-02}	7.59×10^{-02}	7.45×10^{-02}	7.11×10^{-02}	7.57×10^{-02}	7.43×10^{-02}	$< 10^{-100}$	$< 10^{-100}$	$< 10^{-100}$
^{59}Mn	5	7.40×10^{-02}	7.91×10^{-02}	7.78×10^{-02}	7.40×10^{-02}	7.89×10^{-02}	7.78×10^{-02}	3.23×10^{-21}	2.96×10^{-21}	2.99×10^{-21}
	10	5.11×10^{-01}	5.94×10^{-01}	5.31×10^{-01}	5.11×10^{-01}	5.94×10^{-01}	5.31×10^{-01}	2.13×10^{-10}	2.26×10^{-10}	1.95×10^{-10}
	15	$1.51 \times 10^{+00}$	$2.48 \times 10^{+00}$	$1.45 \times 10^{+00}$	$1.51 \times 10^{+00}$	$2.48 \times 10^{+00}$	$1.45 \times 10^{+00}$	8.32×10^{-07}	1.31×10^{-06}	7.31×10^{-07}
	30	$2.28 \times 10^{+00}$	$8.22 \times 10^{+00}$	$2.06 \times 10^{+00}$	$2.28 \times 10^{+00}$	$8.22 \times 10^{+00}$	$2.06 \times 10^{+00}$	2.30×10^{-03}	8.71×10^{-03}	1.99×10^{-03}
	0.1	1.19×10^{-01}	1.07×10^{-01}	1.10×10^{-01}	1.19×10^{-01}	1.07×10^{-01}	1.10×10^{-01}	$< 10^{-100}$	$< 10^{-100}$	$< 10^{-100}$
^{60}Co	1	2.08×10^{-01}	2.07×10^{-01}	2.09×10^{-01}	2.08×10^{-01}	2.07×10^{-01}	2.09×10^{-01}	7.94×10^{-97}	9.20×10^{-97}	8.65×10^{-97}
	5	2.55×10^{-01}	2.63×10^{-01}	2.62×10^{-01}	2.55×10^{-01}	2.63×10^{-01}	2.62×10^{-01}	2.99×10^{-21}	3.42×10^{-21}	3.14×10^{-21}
	10	3.48×10^{-01}	4.11×10^{-01}	4.18×10^{-01}	3.48×10^{-01}	4.11×10^{-01}	4.18×10^{-01}	3.32×10^{-11}	3.77×10^{-11}	3.48×10^{-11}
	15	9.08×10^{-01}	9.08×10^{-01}	9.48×10^{-01}	9.08×10^{-01}	9.08×10^{-01}	9.48×10^{-01}	2.12×10^{-07}	2.08×10^{-07}	1.90×10^{-07}
	30	$4.28 \times 10^{+00}$	$4.03 \times 10^{+00}$	$3.16 \times 10^{+00}$	$4.28 \times 10^{+00}$	$4.03 \times 10^{+00}$	$3.16 \times 10^{+00}$	3.08×10^{-03}	3.18×10^{-03}	2.13×10^{-03}
^{61}Co	0.1	1.75×10^{-48}	2.69×10^{-13}	5.94×10^{-13}	1.37×10^{-48}	2.21×10^{-13}	5.04×10^{-13}	$< 10^{-100}$	$< 10^{-100}$	$< 10^{-100}$
	1	8.07×10^{-10}	1.08×10^{-06}	1.60×10^{-06}	7.45×10^{-10}	9.98×10^{-07}	1.49×10^{-06}	$< 10^{-100}$	$< 10^{-100}$	$< 10^{-100}$
	5	4.61×10^{-05}	1.69×10^{-04}	1.69×10^{-04}	4.60×10^{-05}	1.69×10^{-04}	1.69×10^{-04}	2.81×10^{-27}	8.97×10^{-27}	9.16×10^{-27}
	10	7.98×10^{-04}	1.73×10^{-03}	1.66×10^{-03}	7.98×10^{-04}	1.73×10^{-03}	1.66×10^{-03}	1.35×10^{-14}	2.43×10^{-14}	2.44×10^{-14}
	15	3.61×10^{-03}	6.82×10^{-03}	6.68×10^{-03}	3.60×10^{-03}	6.82×10^{-03}	6.68×10^{-03}	3.21×10^{-10}	5.38×10^{-10}	5.33×10^{-10}
^{61}Fe	30	2.29×10^{-02}	4.04×10^{-02}	3.91×10^{-02}	2.29×10^{-02}	4.04×10^{-02}	3.91×10^{-02}	1.10×10^{-05}	1.87×10^{-05}	1.81×10^{-05}
	0.1	1.97×10^{-07}	$3.28 \times 10^{+00}$	6.43×10^{-07}	1.78×10^{-07}	$3.27 \times 10^{+00}$	6.04×10^{-07}	$< 10^{-100}$	$< 10^{-100}$	$< 10^{-100}$
	1	1.00×10^{-04}	$3.30 \times 10^{+00}$	8.32×10^{-05}	9.73×10^{-05}	$3.30 \times 10^{+00}$	8.07×10^{-05}	$< 10^{-100}$	2.42×10^{-67}	$< 10^{-100}$
	5	1.05×10^{-03}	$5.14 \times 10^{+00}$	8.87×10^{-04}	1.05×10^{-03}	$5.14 \times 10^{+00}$	8.85×10^{-04}	6.61×10^{-26}	3.48×10^{-15}	5.50×10^{-26}
	10	3.40×10^{-03}	$8.71 \times 10^{+00}$	2.61×10^{-03}	3.40×10^{-03}	$8.71 \times 10^{+00}$	2.61×10^{-03}	5.32×10^{-14}	5.79×10^{-08}	4.26×10^{-14}
^{62}Co	15	1.39×10^{-02}	$2.37 \times 10^{+01}$	9.77×10^{-03}	1.38×10^{-02}	$2.37 \times 10^{+01}$	9.77×10^{-03}	1.21×10^{-09}	5.89×10^{-05}	8.85×10^{-10}
	30	9.57×10^{-02}	$1.26 \times 10^{+02}$	6.49×10^{-02}	9.57×10^{-02}	$1.26 \times 10^{+02}$	6.49×10^{-02}	4.82×10^{-05}	2.23×10^{-01}	3.30×10^{-05}
	0.1	9.79×10^{-03}	5.19×10^{-03}	5.71×10^{-03}	9.73×10^{-03}	5.15×10^{-03}	5.68×10^{-03}	$< 10^{-100}$	$< 10^{-100}$	$< 10^{-100}$
	1	1.12×10^{-02}	6.43×10^{-02}	7.03×10^{-02}	1.12×10^{-02}	6.40×10^{-02}	7.00×10^{-02}	$< 10^{-100}$	$< 10^{-100}$	$< 10^{-100}$
	5	5.66×10^{-02}	4.76×10^{-02}	4.94×10^{-02}	5.66×10^{-02}	4.75×10^{-02}	4.94×10^{-02}	3.43×10^{-22}	2.73×10^{-22}	2.74×10^{-22}
^{62}Fe	10	1.56×10^{-01}	1.40×10^{-01}	1.43×10^{-01}	1.56×10^{-01}	1.40×10^{-01}	1.43×10^{-01}	1.12×10^{-11}	8.81×10^{-12}	8.97×10^{-12}
	15	4.56×10^{-01}	4.04×10^{-01}	4.06×10^{-01}	4.56×10^{-01}	4.04×10^{-01}	4.05×10^{-01}	8.89×10^{-08}	7.52×10^{-08}	7.18×10^{-08}
	30	$2.19 \times 10^{+00}$	$2.74 \times 10^{+00}$	$1.79 \times 10^{+00}$	$2.19 \times 10^{+00}$	$2.74 \times 10^{+00}$	$1.79 \times 10^{+00}$	1.49×10^{-03}	2.03×10^{-03}	1.17×10^{-03}
	0.1	4.61×10^{-04}	7.46×10^{-02}	7.52×10^{-02}	4.44×10^{-04}	7.43×10^{-02}	7.50×10^{-02}	$< 10^{-100}$	$< 10^{-100}$	$< 10^{-100}$
	1	1.73×10^{-03}	1.83×10^{-01}	1.85×10^{-01}	1.71×10^{-03}	1.82×10^{-01}	1.84×10^{-01}	$< 10^{-100}$	5.50×10^{-96}	5.58×10^{-96}
^{63}Co	5	1.69×10^{-02}	3.31×10^{-01}	3.33×10^{-01}	1.69×10^{-02}	3.31×10^{-01}	3.33×10^{-01}	3.60×10^{-24}	5.00×10^{-21}	5.41×10^{-21}
	10	5.16×10^{-02}	7.28×10^{-01}	7.21×10^{-01}	5.16×10^{-02}	7.28×10^{-01}	7.21×10^{-01}	1.07×10^{-12}	6.70×10^{-11}	6.93×10^{-11}
	15	1.20×10^{-01}	$1.77 \times 10^{+00}$	$1.77 \times 10^{+00}$	1.20×10^{-01}	$1.77 \times 10^{+00}$	$1.77 \times 10^{+00}$	1.24×10^{-08}	3.94×10^{-07}	3.90×10^{-07}
	30	5.43×10^{-01}	$7.14 \times 10^{+00}$	$5.68 \times 10^{+00}$	5.43×10^{-01}	$7.14 \times 10^{+00}$	$5.68 \times 10^{+00}$	2.88×10^{-04}	5.43×10^{-03}	3.98×10^{-03}
	0.1	7.40×10^{-04}	4.84×10^{-03}	8.07×10^{-04}	7.24×10^{-04}	4.76×10^{-03}	7.91×10^{-04}	$< 10^{-100}$	$< 10^{-100}$	$< 10^{-100}$
^{63}Fe	1	9.91×10^{-04}	4.84×10^{-03}	1.10×10^{-03}	9.79×10^{-04}	4.80×10^{-03}	1.09×10^{-03}	$< 10^{-100}$		

Table 4. Same as Table 1 but for $^{63,65,67}\text{Ni}$, $^{64,65,67}\text{Co}$ and $^{64,66-70}\text{Cu}$.

Nuclei	T	$\rho=10^1$			$\rho=10^5$			$\rho=10^{11}$		
		TF	3TF	5TF	TF	3TF	5TF	TF	3TF	5TF
^{63}Ni	0.1	5.96×10^{-12}	4.54×10^{-12}	4.04×10^{-12}	2.03×10^{-12}	1.58×10^{-12}	1.40×10^{-12}	$< 10^{-100}$	$< 10^{-100}$	$< 10^{-100}$
	1	3.73×10^{-08}	4.84×10^{-08}	3.71×10^{-08}	3.25×10^{-08}	4.24×10^{-08}	3.24×10^{-08}	$< 10^{-100}$	$< 10^{-100}$	$< 10^{-100}$
	5	1.43×10^{-05}	1.35×10^{-05}	1.21×10^{-05}	1.42×10^{-05}	1.35×10^{-05}	1.21×10^{-05}	6.59×10^{-28}	8.83×10^{-28}	7.38×10^{-28}
	10	3.43×10^{-04}	4.03×10^{-04}	2.43×10^{-04}	3.43×10^{-04}	4.03×10^{-04}	2.43×10^{-04}	4.86×10^{-15}	6.46×10^{-14}	3.50×10^{-15}
	15	3.30×10^{-03}	1.02×10^{-02}	2.00×10^{-03}	3.30×10^{-03}	1.02×10^{-02}	2.00×10^{-03}	2.45×10^{-10}	7.19×10^{-09}	1.45×10^{-10}
^{64}Co	0.1	3.30×10^{-02}	7.48×10^{-01}	1.86×10^{-02}	3.30×10^{-02}	7.48×10^{-01}	1.86×10^{-02}	1.52×10^{-05}	9.77×10^{-04}	8.43×10^{-06}
	1	1.36×10^{-01}	2.37×10^{-01}	2.17×10^{-01}	1.35×10^{-01}	2.36×10^{-01}	2.16×10^{-01}	$< 10^{-100}$	$< 10^{-100}$	$< 10^{-100}$
	5	1.56×10^{-01}	2.88×10^{-01}	2.70×10^{-01}	1.56×10^{-01}	2.88×10^{-01}	2.70×10^{-01}	$< 10^{-100}$	6.71×10^{-96}	1.50×10^{-95}
	10	5.51×10^{-01}	$1.06 \times 10^{+00}$	$1.02 \times 10^{+00}$	5.51×10^{-01}	$1.06 \times 10^{+00}$	$1.02 \times 10^{+00}$	1.48×10^{-21}	1.50×10^{-20}	1.50×10^{-20}
	15	8.30×10^{-01}	$2.03 \times 10^{+00}$	$1.88 \times 10^{+00}$	8.30×10^{-01}	$2.03 \times 10^{+00}$	$1.88 \times 10^{+00}$	3.89×10^{-11}	1.67×10^{-10}	1.57×10^{-10}
^{64}Cu	0.1	$1.42 \times 10^{+00}$	$3.80 \times 10^{+00}$	$3.46 \times 10^{+00}$	$1.42 \times 10^{+00}$	$3.80 \times 10^{+00}$	$3.46 \times 10^{+00}$	2.16×10^{-07}	4.76×10^{-07}	6.82×10^{-07}
	1	$4.60 \times 10^{+00}$	$1.09 \times 10^{+01}$	$9.89 \times 10^{+00}$	$4.60 \times 10^{+00}$	$1.09 \times 10^{+01}$	$9.89 \times 10^{+00}$	2.84×10^{-03}	7.21×10^{-03}	6.55×10^{-03}
	5	$< 10^{-100}$	$< 10^{-100}$	$< 10^{-100}$	$< 10^{-100}$	$< 10^{-100}$	$< 10^{-100}$	$< 10^{-100}$	$< 10^{-100}$	$< 10^{-100}$
	10	4.45×10^{-24}	5.55×10^{-18}	1.09×10^{-17}	3.90×10^{-24}	4.65×10^{-18}	9.79×10^{-18}	$< 10^{-100}$	$< 10^{-100}$	$< 10^{-100}$
	15	1.75×10^{-08}	3.53×10^{-08}	5.45×10^{-08}	1.74×10^{-08}	3.53×10^{-08}	5.43×10^{-08}	4.03×10^{-31}	1.03×10^{-30}	1.29×10^{-30}
^{65}Co	0.1	2.46×10^{-06}	5.16×10^{-06}	6.14×10^{-06}	2.45×10^{-06}	5.16×10^{-06}	6.12×10^{-06}	2.91×10^{-17}	4.02×10^{-17}	5.55×10^{-17}
	1	2.02×10^{-05}	1.32×10^{-04}	5.64×10^{-05}	2.02×10^{-05}	4.24×10^{-05}	5.64×10^{-05}	1.54×10^{-12}	2.20×10^{-12}	3.27×10^{-12}
	5	1.99×10^{-04}	3.99×10^{-04}	5.93×10^{-04}	1.99×10^{-04}	3.99×10^{-04}	5.93×10^{-04}	9.18×10^{-08}	1.58×10^{-07}	2.47×10^{-07}
	10	4.80×10^{-01}	4.66×10^{-01}	4.82×10^{-01}	4.79×10^{-01}	4.66×10^{-01}	4.81×10^{-01}	$< 10^{-100}$	$< 10^{-100}$	$< 10^{-100}$
	15	5.71×10^{-01}	5.60×10^{-01}	5.81×10^{-01}	5.70×10^{-01}	5.60×10^{-01}	5.81×10^{-01}	2.07×10^{-92}	8.65×10^{-93}	9.95×10^{-93}
^{65}Ni	0.1	9.51×10^{-01}	8.34×10^{-01}	9.53×10^{-01}	9.51×10^{-01}	8.34×10^{-01}	9.53×10^{-01}	5.21×10^{-20}	2.96×10^{-20}	3.75×10^{-20}
	1	$1.71 \times 10^{+00}$	$1.75 \times 10^{+00}$	$2.06 \times 10^{+00}$	$1.71 \times 10^{+00}$	$1.75 \times 10^{+00}$	$2.06 \times 10^{+00}$	$2.67 \times 10^{+00}$	2.12×10^{-10}	2.62×10^{-10}
	5	$3.85 \times 10^{+00}$	$3.45 \times 10^{+00}$	$4.11 \times 10^{+00}$	$3.85 \times 10^{+00}$	$3.45 \times 10^{+00}$	$4.11 \times 10^{+00}$	1.12×10^{-06}	8.63×10^{-07}	1.04×10^{-06}
	10	$1.18 \times 10^{+01}$	$9.77 \times 10^{+00}$	$9.44 \times 10^{+00}$	$1.18 \times 10^{+01}$	$9.77 \times 10^{+00}$	$9.44 \times 10^{+00}$	9.12×10^{-03}	7.33×10^{-03}	6.93×10^{-03}
	15	3.09×10^{-03}	3.02×10^{-03}	2.84×10^{-03}	3.03×10^{-03}	2.96×10^{-03}	2.79×10^{-03}	$< 10^{-100}$	$< 10^{-100}$	$< 10^{-100}$
^{66}Cu	0.1	3.02×10^{-03}	2.90×10^{-03}	2.67×10^{-03}	2.99×10^{-03}	2.87×10^{-03}	2.65×10^{-03}	$< 10^{-100}$	$< 10^{-100}$	$< 10^{-100}$
	1	4.35×10^{-03}	3.72×10^{-03}	3.87×10^{-03}	4.34×10^{-03}	3.71×10^{-03}	3.86×10^{-03}	8.04×10^{-25}	6.70×10^{-25}	6.76×10^{-25}
	5	1.76×10^{-02}	1.21×10^{-02}	1.58×10^{-02}	1.76×10^{-02}	1.21×10^{-02}	1.58×10^{-02}	6.19×10^{-13}	3.94×10^{-13}	4.62×10^{-13}
	10	1.11×10^{-01}	7.82×10^{-02}	9.14×10^{-02}	1.11×10^{-01}	7.82×10^{-02}	9.12×10^{-02}	1.48×10^{-08}	1.06×10^{-08}	1.07×10^{-08}
	15	8.07×10^{-01}	$1.03 \times 10^{+00}$	6.11×10^{-01}	8.07×10^{-01}	$1.03 \times 10^{+00}$	6.11×10^{-01}	4.71×10^{-04}	6.55×10^{-04}	3.39×10^{-04}
^{67}Co	0.1	6.38×10^{-36}	1.87×10^{-07}	2.21×10^{-07}	1.99×10^{-07}	5.12×10^{-08}	6.59×10^{-08}	$< 10^{-100}$	$< 10^{-100}$	$< 10^{-100}$
	1	1.26×10^{-09}	1.25×10^{-06}	9.89×10^{-07}	1.06×10^{-09}	1.10×10^{-06}	8.55×10^{-07}	$< 10^{-100}$	$< 10^{-100}$	$< 10^{-100}$
	5	2.18×10^{-05}	1.00×10^{-04}	1.09×10^{-04}	2.17×10^{-05}	9.98×10^{-05}	1.09×10^{-04}	4.99×10^{-28}	2.00×10^{-27}	2.09×10^{-27}
	10	2.03×10^{-04}	5.66×10^{-04}	5.66×10^{-04}	2.03×10^{-04}	5.65×10^{-04}	5.66×10^{-04}	2.33×10^{-15}	4.82×10^{-15}	4.62×10^{-15}
	15	8.73×10^{-04}	1.99×10^{-03}	1.95×10^{-03}	8.73×10^{-04}	1.99×10^{-03}	1.94×10^{-03}	6.07×10^{-11}	1.17×10^{-10}	1.13×10^{-10}
^{67}Ni	0.1	5.73×10^{-03}	1.18×10^{-02}	1.17×10^{-02}	5.73×10^{-03}	1.18×10^{-02}	1.17×10^{-02}	2.52×10^{-06}	4.97×10^{-06}	4.92×10^{-06}
	1	$4.94 \times 10^{+00}$	$4.43 \times 10^{+00}$	$4.54 \times 10^{+00}$	$4.94 \times 10^{+00}$	$4.43 \times 10^{+00}$	$4.54 \times 10^{+00}$	$< 10^{-100}$	$< 10^{-100}$	$< 10^{-100}$
	5	$5.14 \times 10^{+00}$	$4.65 \times 10^{+00}$	$4.85 \times 10^{+00}$	$5.14 \times 10^{+00}$	$4.65 \times 10^{+00}$	$4.85 \times 10^{+00}$	8.39×10^{-80}	6.21×10^{-80}	8.05×10^{-80}
	10	$7.11 \times 10^{+00}$	$6.22 \times 10^{+00}$	$6.73 \times 10^{+00}$	$7.11 \times 10^{+00}$	$6.22 \times 10^{+00}$	$6.73 \times 10^{+00}$	2.83×10^{-17}	2.25×10^{-17}	2.82×10^{-17}
	15	$1.07 \times 10^{+01}$	$1.16 \times 10^{+01}$	$1.24 \times 10^{+01}$	$1.07 \times 10^{+01}$	$1.16 \times 10^{+01}$	$1.24 \times 10^{+01}$	9.75×10^{-09}	9.77×10^{-09}	1.78×10^{-08}
^{67}Cu	0.1	$2.22 \times 10^{+01}$	$2.30 \times 10^{+01}$	$2.68 \times 10^{+01}$	$2.22 \times 10^{+01}$	$2.30 \times 10^{+01}$	$2.68 \times 10^{+01}$	1.79×10^{-05}	1.74×10^{-05}	3.62×10^{-05}
	1	$6.27 \times 10^{+01}$	$6.17 \times 10^{+01}$	$7.50 \times 10^{+01}$	$6.27 \times 10^{+01}$	$6.17 \times 10^{+01}$	$7.50 \times 10^{+01}$	7.06×10^{-02}	6.87×10^{-02}	1.17×10^{-01}
	5	2.25×10^{-05}	1.75×10^{-05}	1.72×10^{-05}	1.76×10^{-05}	1.37×10^{-05}	1.35×10^{-05}	$< 10^{-100}$	$< 10^{-100}$	$< 10^{-100}$
	10	3.45×10^{-04}	2.77×10^{-05}	2.87×10^{-05}	3.20×10^{-05}	2.58×10^{-05}	2.67×10^{-05}	$< 10^{-100}$	$< 10^{-100}$	$< 10^{-100}$
	15	2.23×10^{-04}	2.08×10^{-04}	1.98×10^{-04}	2.23×10^{-04}	2.08×10^{-04}	1.97×10^{-04}	5.86×10^{-27}	6.15×10^{-27}	4.12×10^{-27}
^{68}Cu	0.1	8.04×10^{-04}	7.87×10^{-04}	7.48×10^{-04}	8.04×10^{-04}	7.85×10^{-04}	7.48×10^{-04}	1.14×10^{-14}	1.22×10^{-14}	7.87×10^{-15}
	1	3.76×10^{-03}	3.53×10^{-03}	2.95×10^{-03}	3.76×10^{-03}	3.53×10^{-03}	2.95×10^{-03}	3.10×10^{-10}	3.40×10^{-10}	2.00×10^{-10}
	5	3.02×10^{-02}	4.06×10^{-02}	1.77×10^{-02}	3.02×10^{-02}	4.06×10^{-02}	1.77×10^{-02}	1.45×10^{-05}	2.15×10^{-05}	7.91×10^{-06}
	10	2.04×10^{-02}	3.97×10^{-02}	2.55×10^{-02}	2.03×10^{-02}	3.95×10^{-02}	2.54×10^{-02}	$< 10^{-100}$	$< 10^{-100}$	$< 10^{-100}$
	15	4.71×10^{-02}	7.93×10^{-02}	5.98×10^{-02}	4.69×10^{-02}	7.91×10^{-02}	5.97×10^{-02}	$< 10^{-100}$	$< 10^{-100}$	$< 10^{-100}$
^{69}Cu	0.1	5.57×10^{-02}	9.57×10^{-02}	7.45×10^{-02}	5.57×10^{-02}	9.57×10^{-02}	7.45×10^{-02}	1.76×10^{-22}	2.65×10^{-22}	1.46×10^{-22}
	1	1.95×10^{-01}	2.68×10^{-01}	2.21×10^{-01}	1.95×10^{-01}	2.67×10^{-01}	2.21×10^{-01}	2.31×10^{-11}	5.24×10^{-11}	3.30×10^{-11}
	5	$1.21 \times 10^{+00}$	$1.98 \times 10^{+00}$	$1.46 \times 10^{+00}$	$1.21 \times 10^{+00}$	$1.98 \times 10^{+00}$	$1.46 \times 10^{+00}$	2.99×10^{-07}	8.05×10^{-07}	4.62×10^{-07}
	10	$7.52 \times 10^{+00}$	$1.89 \times 10^{+01}$	$1.03 \times 10^{+01}$	$7.52 \times 10^{+00}$	$1.89 \times 10^{+01}$	$1.03 \times 10^{+01}$	5.42×10^{-03}	1.75×10^{-02}	8.22×10^{-03}
	15	2.63×10^{-03}	8.11×10^{-03}	7.69×10^{-03}	2.55×10^{-03}	7.98×10^{-03}	7.57×10^{-03}	$< 10^{-100}$	$< 10^{-100}$	$< 10^{-100}$
^{70}Cu	0.1	3.15×10^{-03}	7.41×10^{-03}	6.8						

Table 5. Same as Table 1 but for ^{71}Cu , $^{73,75-78}\text{Ga}$, ^{73}Zn and $^{77-80}\text{Ge}$.

Nuclei	T	$\rho=10^1$			$\rho=10^5$			$\rho=10^{11}$		
		TF	3TF	5TF	TF	3TF	5TF	TF	3TF	5TF
^{71}Cu	0.1	3.29×10^{-01}	3.20×10^{-01}	3.20×10^{-01}	3.28×10^{-01}	3.18×10^{-01}	3.19×10^{-01}	$< 10^{-100}$	$< 10^{-100}$	$< 10^{-100}$
	1	3.30×10^{-01}	3.21×10^{-01}	3.21×10^{-01}	3.29×10^{-01}	3.21×10^{-01}	3.21×10^{-01}	5.05×10^{-100}	6.41×10^{-100}	6.38×10^{-100}
	5	4.05×10^{-01}	3.64×10^{-01}	3.72×10^{-01}	4.05×10^{-01}	3.64×10^{-01}	3.72×10^{-01}	1.18×10^{-21}	1.05×10^{-21}	1.08×10^{-21}
	10	6.28×10^{-01}	5.60×10^{-01}	5.87×10^{-01}	6.28×10^{-01}	5.60×10^{-01}	5.86×10^{-01}	3.00×10^{-11}	2.90×10^{-11}	2.83×10^{-11}
	30	$1.31 \times 10^{+00}$	$1.13 \times 10^{+00}$	$1.18 \times 10^{+00}$	$1.31 \times 10^{+00}$	$1.13 \times 10^{+00}$	$1.18 \times 10^{+00}$	1.95×10^{-07}	1.96×10^{-07}	1.77×10^{-07}
^{73}Ga	0.1	$4.20 \times 10^{+00}$	$4.30 \times 10^{+00}$	$3.54 \times 10^{+00}$	$4.20 \times 10^{+00}$	$4.30 \times 10^{+00}$	$3.54 \times 10^{+00}$	2.54×10^{-03}	2.99×10^{-03}	2.13×10^{-03}
	1	7.73×10^{-04}	7.60×10^{-04}	7.53×10^{-04}	7.48×10^{-04}	7.38×10^{-04}	7.29×10^{-04}	$< 10^{-100}$	$< 10^{-100}$	$< 10^{-100}$
	5	7.73×10^{-04}	7.62×10^{-04}	7.55×10^{-04}	7.60×10^{-04}	7.50×10^{-04}	7.41×10^{-04}	$< 10^{-100}$	$< 10^{-100}$	$< 10^{-100}$
	10	4.08×10^{-03}	4.23×10^{-03}	4.26×10^{-03}	4.07×10^{-03}	4.23×10^{-03}	4.26×10^{-03}	1.05×10^{-24}	1.04×10^{-24}	9.55×10^{-25}
	30	2.81×10^{-02}	2.63×10^{-02}	2.80×10^{-02}	2.81×10^{-02}	2.63×10^{-02}	2.80×10^{-02}	6.37×10^{-13}	6.53×10^{-13}	5.92×10^{-13}
^{73}Zn	0.1	1.19×10^{-01}	1.14×10^{-01}	1.13×10^{-01}	1.19×10^{-01}	1.14×10^{-01}	1.13×10^{-01}	1.17×10^{-08}	1.37×10^{-08}	1.06×10^{-08}
	1	6.98×10^{-01}	$1.05 \times 10^{+00}$	6.19×10^{-01}	6.98×10^{-01}	$1.05 \times 10^{+00}$	6.19×10^{-01}	3.56×10^{-04}	6.32×10^{-04}	3.11×10^{-04}
	5	1.92×10^{-03}	6.01×10^{-04}	6.00×10^{-04}	1.86×10^{-03}	5.79×10^{-04}	5.77×10^{-04}	$< 10^{-100}$	$< 10^{-100}$	$< 10^{-100}$
	10	4.04×10^{-03}	4.05×10^{-03}	2.00×10^{-03}	3.99×10^{-03}	4.02×10^{-03}	1.97×10^{-03}	$< 10^{-100}$	$< 10^{-100}$	$< 10^{-100}$
	30	1.72×10^{-02}	1.62×10^{-02}	1.61×10^{-02}	1.72×10^{-02}	1.62×10^{-02}	1.61×10^{-02}	7.48×10^{-23}	5.31×10^{-23}	6.87×10^{-23}
^{75}Ga	0.1	1.32×10^{-01}	9.62×10^{-02}	1.13×10^{-01}	1.32×10^{-01}	9.62×10^{-02}	1.13×10^{-01}	1.56×10^{-11}	9.53×10^{-12}	1.11×10^{-11}
	1	9.71×10^{-01}	7.19×10^{-01}	7.91×10^{-01}	9.71×10^{-01}	7.19×10^{-01}	7.91×10^{-01}	2.53×10^{-07}	1.81×10^{-07}	1.84×10^{-07}
	5	$7.66 \times 10^{+00}$	$8.00 \times 10^{+00}$	$6.24 \times 10^{+00}$	$7.66 \times 10^{+00}$	$8.00 \times 10^{+00}$	$6.24 \times 10^{+00}$	5.70×10^{-03}	6.18×10^{-03}	4.47×10^{-03}
	10	1.44×10^{-02}	1.37×10^{-02}	1.36×10^{-02}	1.43×10^{-02}	1.36×10^{-02}	1.35×10^{-02}	$< 10^{-100}$	$< 10^{-100}$	$< 10^{-100}$
	30	1.44×10^{-02}	1.37×10^{-02}	1.36×10^{-02}	1.44×10^{-02}	1.36×10^{-02}	1.36×10^{-02}	$< 10^{-100}$	$< 10^{-100}$	$< 10^{-100}$
^{76}Ga	0.1	4.43×10^{-02}	8.55×10^{-02}	9.79×10^{-02}	4.41×10^{-02}	8.53×10^{-02}	9.75×10^{-02}	$< 10^{-100}$	$< 10^{-100}$	$< 10^{-100}$
	1	5.75×10^{-02}	1.03×10^{-01}	1.01×10^{-01}	5.73×10^{-02}	1.03×10^{-01}	1.01×10^{-01}	$< 10^{-100}$	2.99×10^{-99}	1.29×10^{-98}
	5	1.47×10^{-01}	2.19×10^{-01}	2.21×10^{-01}	1.47×10^{-01}	2.19×10^{-01}	2.21×10^{-01}	9.02×10^{-22}	3.98×10^{-21}	5.32×10^{-21}
	10	4.36×10^{-01}	8.22×10^{-01}	8.20×10^{-01}	4.36×10^{-01}	8.20×10^{-01}	8.20×10^{-01}	3.71×10^{-11}	1.14×10^{-10}	1.25×10^{-10}
	30	$1.25 \times 10^{+00}$	$2.80 \times 10^{+00}$	$2.79 \times 10^{+00}$	$1.25 \times 10^{+00}$	$2.80 \times 10^{+00}$	$2.79 \times 10^{+00}$	2.70×10^{-07}	8.13×10^{-07}	8.45×10^{-07}
^{77}Ga	0.1	$6.32 \times 10^{+00}$	$1.47 \times 10^{+01}$	$1.48 \times 10^{+01}$	$6.32 \times 10^{+00}$	$1.47 \times 10^{+01}$	$1.48 \times 10^{+01}$	4.35×10^{-03}	1.15×10^{-02}	1.16×10^{-02}
	1	7.10×10^{-02}	6.22×10^{-02}	6.08×10^{-02}	7.06×10^{-02}	6.21×10^{-02}	6.07×10^{-02}	$< 10^{-100}$	$< 10^{-100}$	$< 10^{-100}$
	5	7.10×10^{-02}	6.22×10^{-02}	6.08×10^{-02}	7.08×10^{-02}	6.21×10^{-02}	6.07×10^{-02}	4.94×10^{-97}	4.95×10^{-97}	4.20×10^{-97}
	10	5.64×10^{-01}	5.92×10^{-01}	6.65×10^{-01}	5.64×10^{-01}	5.92×10^{-01}	6.65×10^{-01}	9.38×10^{-11}	8.41×10^{-11}	8.63×10^{-11}
	30	$2.18 \times 10^{+00}$	$1.93 \times 10^{+00}$	$2.29 \times 10^{+00}$	$2.18 \times 10^{+00}$	$1.93 \times 10^{+00}$	$2.29 \times 10^{+00}$	6.65×10^{-07}	5.69×10^{-07}	5.87×10^{-07}
^{77}Ge	0.1	1.37×10^{-04}	1.18×10^{-04}	1.20×10^{-04}	1.29×10^{-04}	1.10×10^{-04}	1.12×10^{-04}	$< 10^{-100}$	$< 10^{-100}$	$< 10^{-100}$
	1	2.39×10^{-04}	2.84×10^{-04}	2.38×10^{-04}	2.35×10^{-04}	2.84×10^{-04}	2.33×10^{-04}	$< 10^{-100}$	$< 10^{-100}$	$< 10^{-100}$
	5	5.07×10^{-03}	3.84×10^{-03}	5.26×10^{-03}	5.07×10^{-03}	3.84×10^{-03}	5.26×10^{-03}	5.89×10^{-24}	3.48×10^{-24}	4.98×10^{-24}
	10	7.57×10^{-02}	4.73×10^{-02}	6.98×10^{-02}	7.50×10^{-02}	4.73×10^{-02}	6.98×10^{-02}	5.33×10^{-12}	2.99×10^{-12}	4.32×10^{-12}
	30	6.14×10^{-01}	3.98×10^{-01}	5.46×10^{-01}	6.14×10^{-01}	3.98×10^{-01}	5.46×10^{-01}	1.16×10^{-07}	7.55×10^{-08}	9.55×10^{-08}
^{78}Ga	0.1	$4.86 \times 10^{+00}$	$4.31 \times 10^{+00}$	$4.22 \times 10^{+00}$	$4.86 \times 10^{+00}$	$4.31 \times 10^{+00}$	$4.22 \times 10^{+00}$	3.19×10^{-03}	2.93×10^{-03}	2.69×10^{-03}
	1	8.97×10^{-02}	2.44×10^{-01}	2.33×10^{-01}	8.93×10^{-02}	2.44×10^{-01}	2.32×10^{-01}	$< 10^{-100}$	$< 10^{-100}$	$< 10^{-100}$
	5	9.10×10^{-02}	2.48×10^{-01}	2.37×10^{-01}	9.08×10^{-02}	2.47×10^{-01}	2.36×10^{-01}	2.42×10^{-96}	1.34×10^{-91}	8.79×10^{-92}
	10	2.45×10^{-01}	4.01×10^{-01}	4.00×10^{-01}	2.45×10^{-01}	4.01×10^{-01}	3.99×10^{-01}	9.86×10^{-21}	8.45×10^{-20}	7.52×10^{-20}
	30	8.49×10^{-01}	$1.67 \times 10^{+00}$	$1.57 \times 10^{+00}$	8.49×10^{-01}	$1.67 \times 10^{+00}$	$1.57 \times 10^{+00}$	1.49×10^{-10}	6.40×10^{-10}	5.68×10^{-10}
^{78}Ge	0.1	$2.42 \times 10^{+00}$	$6.05 \times 10^{+00}$	$5.51 \times 10^{+00}$	$2.42 \times 10^{+00}$	$6.05 \times 10^{+00}$	$5.50 \times 10^{+00}$	7.74×10^{-07}	3.11×10^{-06}	2.74×10^{-07}
	1	$1.14 \times 10^{+01}$	$3.24 \times 10^{+01}$	$2.85 \times 10^{+01}$	$1.14 \times 10^{+01}$	$3.24 \times 10^{+01}$	$2.85 \times 10^{+01}$	9.02×10^{-03}	3.10×10^{-02}	2.71×10^{-02}
	5	2.88×10^{-07}	2.83×10^{-07}	2.80×10^{-07}	2.73×10^{-07}	2.02×10^{-07}	2.03×10^{-07}	$< 10^{-100}$	$< 10^{-100}$	$< 10^{-100}$
	10	2.87×10^{-07}	2.83×10^{-07}	2.79×10^{-07}	2.84×10^{-07}	2.54×10^{-07}	2.51×10^{-07}	$< 10^{-100}$	$< 10^{-100}$	$< 10^{-100}$
	30	2.01×10^{-04}	1.52×10^{-04}	1.64×10^{-04}	2.01×10^{-04}	1.52×10^{-04}	1.64×10^{-04}	1.03×10^{-24}	1.74×10^{-24}	1.18×10^{-24}
^{79}Ge	0.1	3.89×10^{-02}	5.36×10^{-02}	4.17×10^{-02}	3.89×10^{-02}	5.36×10^{-02}	4.17×10^{-02}	3.61×10^{-12}	1.17×10^{-11}	4.23×10^{-12}
	1	2.12×10^{-01}	5.36×10^{-01}	2.40×10^{-01}	2.12×10^{-01}	5.36×10^{-01}	2.40×10^{-01}	4.90×10^{-08}	3.29×10^{-07}	5.78×10^{-08}
	5	6.35×10^{-01}	$5.55 \times 10^{+00}$	7.10×10^{-01}	6.35×10^{-01}	$5.55 \times 10^{+00}$	7.10×10^{-01}	4.59×10^{-04}	8.89×10^{-03}	5.19×10^{-04}
	10	9.10×10^{-04}	7.11×10^{-04}	7.55×10^{-04}	8.85×10^{-04}	6.90×10^{-04}	7.33×10^{-04}	$< 10^{-100}$	$< 10^{-100}$	$< 10^{-100}$
	30	1.42×10^{-03}	1.02×10^{-03}	1.08×10^{-03}	1.41×10^{-03}	1.00×10^{-03}	1.07×10^{-03}	$< 10^{-100}$	$< 10^{-100}$	$< 10^{-100}$
^{80}Ge	0.1	9.91×10^{-03}	8.79×10^{-03}	8.73×10^{-03}	9.91×10^{-03}	8.79×10^{-03}	8.73×10^{-03}	1.31×10^{-22}	9.66×10^{-23}	1.09×10^{-22}
	1	1.56×10^{-01}	1.37×10^{-01}	1.49×10^{-01}	1.56×10^{-01}	1.37×10^{-01}	1.49×10^{-01}	2.08×10^{-11}	1.75×10^{-11}	1.90×10^{-11}
	5	$1.16 \times 10^{+00}$	9.82×10^{-01}	$1.10 \times 10^{+00}$	$1.16 \times 10^{+00}$	9.82×10^{-01}	$1.10 \times 10^{+00}$	3.14×10^{-07}	2.74×10^{-07}	2.88×10^{-07}
	10	$9.59 \times 10^{+00}$	$9.44 \times 10^{+00}$	$8.79 \times 10^{+00}$	$9.59 \times 10^{+00}$	$9.44 \times 10^{+00}$	$8.79 \times 10^{+00}$	7.23×10^{-03}	7.41×10^{-03}	6.55×10^{-03}
	30	1.17×10^{-04}	1.35×10^{-04}	1.37×10^{-04}	1.07×10^{-04}	1.23×10^{-04}	1.25×10^{-04}	$< 10^{-100}$	$< 10^{-100}$	$< 10^{-100}$

Table 6. Same as Table 1 but for ^{81}Ge , $^{82,83}\text{As}$, ^{83}Se and ^{85}Br .

Nuclei	T	$\rho=10^1$			$\rho=10^5$			$\rho=10^{11}$		
		TF	3TF	5TF	TF	3TF	5TF	TF	3TF	5TF
^{81}Ge	0.1	1.13×10^{-02}	1.00×10^{-02}	1.01×10^{-02}	1.11×10^{-02}	9.89×10^{-03}	9.93×10^{-03}	$< 10^{-100}$	$< 10^{-100}$	$< 10^{-100}$
	1	1.36×10^{-02}	1.25×10^{-02}	1.26×10^{-02}	1.36×10^{-02}	1.24×10^{-02}	1.26×10^{-02}	6.84×10^{-02}	6.55×10^{-92}	7.06×10^{-92}
	5	3.09×10^{-02}	3.12×10^{-02}	3.23×10^{-02}	3.09×10^{-02}	3.12×10^{-02}	3.23×10^{-02}	1.77×10^{-20}	1.45×10^{-20}	1.52×10^{-20}
	10	4.21×10^{-01}	4.16×10^{-01}	4.16×10^{-01}	4.21×10^{-01}	4.16×10^{-01}	4.16×10^{-01}	2.42×10^{-10}	2.16×10^{-10}	2.05×10^{-10}
	15	$3.06 \times 10^{+00}$	$3.08 \times 10^{+00}$	$2.85 \times 10^{+00}$	$3.06 \times 10^{+00}$	$3.08 \times 10^{+00}$	$2.85 \times 10^{+00}$	1.85×10^{-06}	1.84×10^{-06}	1.59×10^{-06}
^{82}As	30	$2.64 \times 10^{+01}$	$3.05 \times 10^{+01}$	$2.38 \times 10^{+01}$	$2.64 \times 10^{+01}$	$3.05 \times 10^{+01}$	$2.38 \times 10^{+01}$	2.68×10^{-02}	3.15×10^{-02}	2.33×10^{-02}
	0.1	2.07×10^{-02}	2.80×10^{-02}	2.39×10^{-02}	2.05×10^{-02}	2.77×10^{-02}	2.37×10^{-02}	$< 10^{-100}$	$< 10^{-100}$	$< 10^{-100}$
	1	2.12×10^{-02}	2.83×10^{-02}	2.43×10^{-02}	2.11×10^{-02}	2.82×10^{-02}	2.42×10^{-02}	4.75×10^{-99}	1.65×10^{-97}	5.51×10^{-97}
	5	3.76×10^{-02}	4.94×10^{-02}	4.53×10^{-02}	3.75×10^{-02}	4.94×10^{-02}	4.53×10^{-02}	1.08×10^{-21}	2.13×10^{-21}	2.16×10^{-21}
	10	3.01×10^{-01}	3.97×10^{-01}	3.84×10^{-01}	3.01×10^{-01}	3.97×10^{-01}	3.84×10^{-01}	5.31×10^{-11}	8.87×10^{-11}	8.77×10^{-11}
^{83}As	15	$1.51 \times 10^{+00}$	$2.12 \times 10^{+00}$	$2.07 \times 10^{+00}$	$1.51 \times 10^{+00}$	$2.12 \times 10^{+00}$	$2.07 \times 10^{+00}$	4.62×10^{-07}	7.55×10^{-07}	7.45×10^{-07}
	30	$1.02 \times 10^{+01}$	$1.42 \times 10^{+01}$	$1.42 \times 10^{+01}$	$1.02 \times 10^{+01}$	$1.42 \times 10^{+01}$	$1.42 \times 10^{+01}$	7.83×10^{-03}	1.16×10^{-02}	1.16×10^{-02}
	0.1	3.13×10^{-02}	3.19×10^{-02}	3.01×10^{-02}	3.11×10^{-02}	3.17×10^{-02}	2.99×10^{-02}	$< 10^{-100}$	$< 10^{-100}$	$< 10^{-100}$
	1	3.18×10^{-02}	3.25×10^{-02}	3.06×10^{-02}	3.17×10^{-02}	3.24×10^{-02}	3.05×10^{-02}	2.39×10^{-94}	2.71×10^{-94}	3.16×10^{-94}
	5	3.49×10^{-02}	2.89×10^{-02}	3.49×10^{-02}	3.48×10^{-02}	2.89×10^{-02}	3.49×10^{-02}	1.18×10^{-20}	8.89×10^{-21}	1.27×10^{-20}
^{83}Se	10	3.08×10^{-01}	2.31×10^{-01}	2.91×10^{-01}	3.08×10^{-01}	2.31×10^{-01}	2.91×10^{-01}	1.44×10^{-10}	1.20×10^{-10}	1.29×10^{-10}
	15	$2.64 \times 10^{+00}$	$2.10 \times 10^{+00}$	$2.41 \times 10^{+00}$	$2.64 \times 10^{+00}$	$2.10 \times 10^{+00}$	$2.41 \times 10^{+00}$	1.30×10^{-06}	1.20×10^{-06}	1.10×10^{-06}
	30	$2.57 \times 10^{+01}$	$2.70 \times 10^{+01}$	$2.31 \times 10^{+01}$	$2.57 \times 10^{+01}$	$2.70 \times 10^{+01}$	$2.31 \times 10^{+01}$	2.35×10^{-02}	2.67×10^{-02}	2.03×10^{-02}
	0.1	2.73×10^{-04}	2.36×10^{-04}	2.33×10^{-04}	2.60×10^{-04}	2.24×10^{-04}	2.21×10^{-04}	$< 10^{-100}$	$< 10^{-100}$	$< 10^{-100}$
	1	5.16×10^{-04}	5.24×10^{-04}	5.50×10^{-04}	5.08×10^{-04}	5.15×10^{-04}	5.41×10^{-04}	$< 10^{-100}$	$< 10^{-100}$	$< 10^{-100}$
^{85}Br	5	3.60×10^{-03}	4.72×10^{-03}	5.28×10^{-03}	3.60×10^{-03}	4.72×10^{-03}	5.27×10^{-03}	5.81×10^{-23}	5.31×10^{-23}	5.35×10^{-23}
	10	1.11×10^{-01}	1.00×10^{-01}	1.19×10^{-01}	1.11×10^{-01}	1.00×10^{-01}	1.19×10^{-01}	1.43×10^{-11}	1.11×10^{-11}	1.23×10^{-11}
	15	9.48×10^{-01}	7.52×10^{-01}	8.65×10^{-01}	9.48×10^{-01}	7.52×10^{-01}	8.65×10^{-01}	2.42×10^{-07}	1.77×10^{-07}	1.92×10^{-07}
	30	$8.83 \times 10^{+00}$	$7.06 \times 10^{+00}$	$7.01 \times 10^{+00}$	$8.83 \times 10^{+00}$	$7.06 \times 10^{+00}$	$7.01 \times 10^{+00}$	6.41×10^{-03}	5.02×10^{-03}	4.80×10^{-03}
	0.1	5.41×10^{-06}	8.02×10^{-06}	6.15×10^{-06}	4.51×10^{-06}	6.82×10^{-06}	5.15×10^{-06}	$< 10^{-100}$	$< 10^{-100}$	$< 10^{-100}$
^{85}Br	1	1.86×10^{-05}	3.24×10^{-05}	2.25×10^{-05}	1.77×10^{-05}	3.10×10^{-05}	2.15×10^{-05}	$< 10^{-100}$	$< 10^{-100}$	$< 10^{-100}$
	5	1.13×10^{-03}	9.51×10^{-04}	1.31×10^{-03}	1.13×10^{-03}	9.48×10^{-04}	1.31×10^{-03}	1.64×10^{-23}	1.12×10^{-23}	1.52×10^{-23}
	10	6.28×10^{-02}	3.74×10^{-02}	5.78×10^{-02}	6.28×10^{-02}	3.74×10^{-02}	5.78×10^{-02}	5.64×10^{-12}	3.91×10^{-12}	4.80×10^{-12}
	15	6.78×10^{-01}	4.45×10^{-01}	6.11×10^{-01}	6.78×10^{-01}	4.44×10^{-01}	6.10×10^{-01}	1.26×10^{-07}	9.77×10^{-08}	1.08×10^{-07}
	30	$6.22 \times 10^{+00}$	$5.79 \times 10^{+00}$	$5.68 \times 10^{+00}$	$6.22 \times 10^{+00}$	$5.79 \times 10^{+00}$	$5.68 \times 10^{+00}$	3.92×10^{-03}	4.02×10^{-03}	3.50×10^{-03}

Table 7. Average β -decay rates calculated using different pairing gap values for limiting physical conditions stated in the heading. The stellar core temperature is given in units of GK and densities in units of gcm^{-3} .

Pairing Gap	T=0.1, $\rho Y_e=10$	T=30, $\rho Y_e=10^{11}$	T=30, $\rho Y_e=10$
TF	1.41×10^{-01}	5.07×10^{-03}	5.75
3TF	2.02×10^{-01}	1.15×10^{-02}	9.95
5TF	1.39×10^{-01}	6.23×10^{-03}	6.34

4. Conclusions and Summary

In this study, we re-examined the influence of pairing gaps on charge-changing transitions, partial half-lives, branching ratios and β -decay rates, for top-ranked 50 nuclei having astrophysical significance. Pairing gaps are one of the most important model parameters in the pn-QRPA approach for calculation of β -decay rates. In order to investigate the effect of pairing gaps on calculated GT strength distributions and half-lives, we used three different empirically calculated values (referred to as TF, 3TF and 5TF). Changing pairing gap values led to significant alterations in the total GT strength and β -decay rates. It was concluded that the 3TF pairing gaps resulted in the best prediction of β -decay half-lives. Following main conclusions are drawn from the current investigation:

- ⊙ The available empirical formulae for pairing gaps give values of Δ_{pp} differing by 0.5 MeV or more. The difference in Δ_{nn} is more than 1 MeV.
- ⊙ The total GT strength changes by orders of magnitude and the placement of GT centroid by up to an order of magnitude or more as the pairing gap values change. The 3TF pairing gap leads to lower placement of GT centroid and higher total GT strength.
- ⊙ The 3TF scheme gives the best predictive power to the current pn-QRPA model.
- ⊙ The 3TF pairing gaps result in biggest stellar β -decay rates for the selected top-50 ranked nuclei.

Author Contributions: J.-U. Nabi and M. Riaz had major contributions. A. Mehmood helped with running servers, drawing tables and figures.

Funding: No funding received.

Institutional Review Board Statement: Not Applicable.

Data Availability Statement: Not applicable.

Acknowledgments: Authors would like to acknowledge the support of the Higher Education Commission Pakistan through Project # 20-15394/NRPU/R&D/HEC/2021

Conflicts of Interest: The authors declare no conflict of interest.

Abbreviations

The following abbreviations are used.

pn-QRPA	proton-neutron quasi-particle random-phase approximation
GT	Gamow-Teller
TF	Traditional Formula
3TF	3 Term Formula
5TF	5 Term Formula

References

- Nabi, J. U. Ullah, A. Khan, A. A. Investigation of important weak interaction nuclei in presupernova evolution. *Astrophys. J.* **2021**, 911(2), 93.
- Bethe, H. A. Supernova mechanisms. *Rev. Mod. Phys.* **1990**, 62 (4), 801.
- Langanke, K., Martínez-Pinedo, G. Nuclear weak-interaction processes in stars. *Rev. Mod. Phys.* **2003**, 75(3), 819.
- Janka, H. T. Langanke, K. Marek, A. Martínez-Pinedo, G. Müller, B. Theory of core-collapse supernovae. *Phys. Rep.* **2007**, 442(1-6), 38-74.
- Bethe, H. A. Brown, G. E. Applegate, J. Lattimer, J. M. Equation of state in the gravitational collapse of stars. *Nucl. Phys. A.* **1979**, 324(2-3), 487-533.
- Niu, Z. M. Liang, H. Z. Nuclear mass predictions with machine learning reaching the accuracy required by r-process studies. *Phys. Rev. C.* **2022**, 106(2), L021303.
- Burbidge, E. M. Burbidge, G. R. Fowler, W. A. Hoyle, F. Synthesis of the elements in stars. *Rev. Mod. Phys.* **1957**, 29(4), 547.
- Smartt, S. Chen, T. W. Jerkstrand, A. Coughlin, M. Kankare, E. Sim, S. A. Yaron, O. A kilonova as the electromagnetic counterpart to a gravitational-wave source. *Nature.* **2017**, 551(7678), 75-79.
- Watson, D. Hansen, C. J. Selsing, J. Koch, A. Malesani, D. B. Andersen, A. C. Pian, E. Identification of strontium in the merger of two neutron stars. *Nature.* **2019**, 574(7779), 497-500.
- Siegel, D. M. Barnes, J. Metzger, B. D. Collapsars as a major source of r-process elements. *Nature.* **2019**, 569(7755), 241-244.
- Borzov, I. N. Beta-decay rates. *Nucl. Phys. A.* **2006**, 777(17), 645-675.
- Panov, I. V. Lutostansky, Y. S. Thielemann, F. K. Beta-decay half-lives for the r-process nuclei. *Nucl. Phys. A.* **2016**, 947, 1-11.
- Takahashi, K. Yamada, M. Kondoh, T. β -decay half-lives calculated on the gross theory. *At. Data Nucl. Data Tab.* **1973**, 12, 101-142.
- Nomura, K. Rodríguez-Guzmán, R. Robledo, L. M. β -decay of even-A nuclei within the interacting boson model with input based on nuclear density functional theory. *Phys. Rev. C* **2020**, 101, 044318.
- Engel, J. Bender, M. Dobaczewski, J. Nazarewicz, W. Surman, R. β -decay rates of r-process waiting-point nuclei in a self-consistent approach. *Phys. Rev. C*, **1999**, 60(1), 014302.
- Kumar, A. Srivastava, P. C. Suzuki, T. Shell model results for nuclear β -decay properties of sd-shell nuclei. *Prog. Theor. Exp. Phys.*, **2020**, 3, 033D01.
- Hix, W. R. Messer, O. E. B. Mezzacappa, A. Liebendörfer, M. Sampaio, J. Langanke, K. Martínez-Pinedo, G. Consequences of nuclear electron capture in core collapse supernovae. *Phys. Rev. Lett.* **2003**, 91(20), 201102.
- Fuller, G. M. Fowler, W. A. Newman, M. J. Stellar weak-interaction rates for sd-shell nuclei. I-Nuclear matrix element systematics with application to Al-26 and selected nuclei of importance to the supernova problem. *Astrophys. J. Suppl. Ser.* **1980**, 42, 447-473.
- Möller, P. Randrup, J. New developments in the calculation of β -strength functions. *Nucl. Phys. A.* **1990**, 514(1), 1-48.

20. Nabi, J. U. Klapdor-Kleingrothaus, H. V. Weak interaction rates of sd-shell nuclei in stellar environments calculated in the proton-neutron quasiparticle random-phase approximation. *At. Data Nucl. Data. Tab.*, **1999**, *71*, 149.
21. Nabi, J. U. Klapdor-Kleingrothaus, H. V. Microscopic calculations of stellar weak interaction rates and energy losses for fp-and fpg-shell nuclei. *At. Data Nucl. Data. Tab.*, **2004**, *88(2)*, 237-476.
22. Nabi, J. U. Riaz, M. Bayram, T. Azaz, M. Effect of Nuclear Deformation on Gamow teller Strength Distributions of Hg Isotopes. *Braz. J. Phys.* **2022**, *52(5)*, 161.
23. Ullah, A. Nabi, J. U. Stellar Weak Rates and Mass Fractions of 20 Most Important fp-shell Nuclei with $A < 65$. *Braz. J. Phys.* **2022**, *52:13*, 1.326.
24. Ullah, A. Nabi, J. U. Tahir, M. Investigation of effects of pairing correlations on calculated β -decay half-lives of fp-shell nuclei. *Braz. J. Phys.* **2023**, *53*, 39.
25. Ha, E. Cheoun, M-K. Sagawa, H. Tensor force effect on pairing correlation for the Gamow-Teller transitions in ^{42}Ca , ^{46}Ti , and ^{10}O . *Prog. Theor. Exp. Phys* **2022**, *043*, D01.
26. Hirsch, M., Staudt, A. Muto, K. Klapdor-Kleingrothaus, H. V. Microscopic predictions of β^+ /EC-decay half-lives. *At. Data. Nucl. Data. Tab.* **1993**, *53(2)*, 165-193.
27. Jensen, A.S. Hansen, P.G. Jonson, B. New mass relations and two-and four-nucleon correlations. *Nucl. Phys. A.* **1984**, *431(3)*, 393-418.
28. Satuła, W. Dobaczewski, J. Nazarewicz, W. Odd-even staggering of nuclear masses: Pairing or shape effect. *Phys. rev. lett.* **1998**, *81(17)*, 3599.
29. Bender, M. Rutz, K. Reinhard, P. G. Maruhn, J. A. Pairing gaps from nuclear mean-field models. *Euro. Phys. J. A.* **2000**, *8*, 59-75.
30. Magner, A. G. Sanzhur, A. I. Fedotkin, S. N. Levon, A. I. Grygoriev, U. V. Shlomo, S. Paring correlations within the micro-macroscopic approach for the level density. **2023**, *2308*, 07784.
31. Lindhard, J. Scharff, M. Binding states of individual nucleons in strongly deformed nuclei. *Mat. Fys. Medd. Dan. Vid. Selsk.* **1955**, *28*, 1-68.
32. Möller, P. Sierk, A. J. Ichikawa, T. Sagawa, H. Nuclear ground-state masses and deformations: FRDM (2012). *At. Data. Nucl. Data. Tab.* **2016**, *109*, 1-204.
33. Ragnarsson, I. Sheline, R. K. Systematics of nuclear deformations. *Phys. Scr.* **1984**, *29(5)*, 385.
34. Kondev, F. G. Wang, M., Huang, W. J. Naimi, S. Audi, G. The NUBASE2020 evaluation of nuclear physics properties. *Chin. Phys. C.* **2021**, *45(3)*, 030001.
35. Staudt, A. Bender, E. Muto, K. Klapdor-Kleingrothaus, H. V. Second-generation microscopic predictions of beta-decay half-lives of neutron-rich nuclei. *At. Data. Nucl. Data. Tab.* **1990**, *44(1)*, 79-132.
36. Homma, H. Bender, E. Hirsch, M. Muto, K. Klapdor-Kleingrothaus, H. V. Oda, T. Systematic study of nuclear β decay. *Phys. Rev.* **1996**, *C 54*, 2972.
37. Wang, M. Huang, W. J. Kondev, F. G. Audi, G. Naimi, S. The AME 2020 atomic mass evaluation (II). Tables, graphs and references. *Chin. Phys. C.*, **2021** *45(3)*, 030003.
38. Muto, K. Bender, E. Klapdor-Kleingrothaus, H. V. Effects of ground-state correlations on $2\nu\beta\beta$ decay rates and limitations of the QRPA approach. *Z. Phys. A. Atom. Nucl.* **1989**, *334*, 177-186.
39. Hirsch, M. Staudt, A. Muto, K. Klapdor-Kleingrothaus, H. V. *Nucl. Phys. A.* **1991**, *535(1)*, 62-76.
40. Hardy, J. C. Towner, I. S. Superallowed $0^+ \rightarrow 0^+$ nuclear β decays: A new survey with precision tests of the conserved vector current hypothesis and the standard model. *Phys. Rev. C.* **2009**, *79(5)*, 055502.
41. Muto, K. Bender, E. Oda, T. Klapdor-Kleingrothaus, H. V. Proton-neutron quasiparticle RPA with separable Gamow-Teller forces. *Z. Phys. A. Hadr. Nucl.* **1992**, *341(4)*, 407-415.
42. Gove, N. B. Martin, M. J. LOG-f Tables for Beta Decay. *At. Data. Nucl. Data. Tab.* **1971**, *(10)*, 205.

Disclaimer/Publisher's Note: The statements, opinions and data contained in all publications are solely those of the individual author(s) and contributor(s) and not of MDPI and/or the editor(s). MDPI and/or the editor(s) disclaim responsibility for any injury to people or property resulting from any ideas, methods, instructions or products referred to in the content.